ISG15 blocks cardiac glycolysis and ensures sufficient mitochondrial energy production during Coxsackievirus B3 infection

Clara Bredow[1] PhD, Fabien Thery[2,3] PhD, Eva Katrin Wirth[4,10] PhD, Sarah Ochs[1] MSc, Meike Kespohl[1,4] PhD, Gunnar Kleinau[7] PhD, Nicolas Kelm[1], Niclas Gimber[5] PhD, Jan Schmoranzer[5] PhD, Martin Voss[1] PhD, Karin Klingel[6] MD/PhD, Joachim Spranger[4,10] MD/PhD, Kostja Renko[18] PhD, Markus Ralser[12] PhD, Michael Mülleder[12] PhD, Arnd Heuser[16] MD, Klaus-Peter Knobeloch[11,17] PhD, Patrick Scheerer[4,7] PhD, Jennifer Kirwan,[13,14,15] PhD, Ulrike Brüning[13,14,15] PhD, Nikolaus Berndt[9] PhD, Francis Impens[2,3,8] PhD, and Antje Beling[1,4,*] MD/PhD

*corresponding author

1 Charité – Universitätsmedizin Berlin, corporate member of Freie Universität Berlin and Humboldt-Universität zu Berlin, Institute of Biochemistry, Berlin, Germany
2 Department of Biomolecular Medicine, Ghent University, Ghent, Belgium
3 VIB-UGent Center for Medical Biotechnology, Ghent, Belgium
4 Deutsches Zentrum für Herz-Kreislauf-Forschung, partner site Berlin, Berlin, Germany
5 Charité – Universitätsmedizin Berlin, corporate member of Freie Universität Berlin and Humboldt-Universität zu Berlin, Advanced Medical Bioimaging Core Facility, Berlin, Germany
6 University of Tübingen, Cardiopathology, Institute for Pathology and Neuropathology, Tübingen, Germany
7 Charité – Universitätsmedizin Berlin, corporate member of Freie Universität Berlin and Humboldt-Universität zu Berlin, Institute of Medical Physics and Biophysics, Group Protein X-ray Crystallography and Signal Transduction, Charitéplatz 1, Berlin, Germany
8 VIB Proteomics Core, Ghent, Belgium
9 Charité – Universitätsmedizin Berlin, corporate member of Freie Universität Berlin and Humboldt-Universität zu Berlin, Institute for Computational and Imaging Science in Cardiovascular Medicine, Berlin, Germany

10 Charité – Universitätsmedizin Berlin, corporate member of Freie Universität Berlin and Humboldt-Universität zu Berlin, Department of Endocrinology, Diabetes and Nutrition, Berlin, Germany
11 University of Freiburg, Institute of Neuropathology, Freiburg, Germany
12 Charité – Universitätsmedizin Berlin, corporate member of Freie Universität Berlin and Humboldt-Universität zu Berlin, Core Facility - High-Throughput Mass Spectrometry, Berlin, Germany
13 Berlin Institute of Health (BIH) @ Charité, Metabolomics Platform, Berlin, Germany
14 Max-Delbrück-Center (MDC) for Molecular Medicine, Berlin, Germany
15 Berlin Institute of Health (BIH), Berlin, Germany
16 Animal Phenotyping Platform, Max-Delbrueck-Center for Molecular Medicine, Berlin, Germany
17 CIBSS – Centre for Integrative Biological Signalling Studies, University of Freiburg, Freiburg, Germany
18 German Federal Institute for Risk Assessment (BfR), German Centre for the Protection of Laboratory Animals (Bf3R), Berlin, Germany

Short title: Remodeling of cardiac metabolism by ISG15

Category: Original article

Total word count: 9500

*__Corresponding author__
Prof. Dr. Antje Beling
Phone: 0049 30 450 528 187
Fax: 0049 30 450 528 921
Email: antje.beling@charite.de
Charité – Universitätsmedizin Berlin
Institute of Biochemistry
Charitéplatz 1
10117 Berlin
Germany

Abstract

Aims: Virus infection triggers inflammation and, may impose nutrient shortage to the heart. Supported by type I interferon (IFN) signaling, cardiomyocytes counteract infection by various effector processes, with the IFN-stimulated gene of 15 kDa (ISG15) system being intensively regulated and protein modification with ISG15 protecting mice Coxsackievirus B3 (CVB3) infection. The underlying molecular aspects how the ISG15 system affects the functional properties of respective protein substrates in the heart are unknown.

Methods and Results: Based on the protective properties due to protein ISGylation, we set out a study investigating CVB3-infected mice in depth and found cardiac atrophy with lower cardiac output in ISG15$^{-/-}$ mice. By mass spectrometry, we identified the protein targets of the ISG15 conjugation machinery in heart tissue and explored how ISGylation affects their function. The cardiac ISGylome showed a strong enrichment of ISGylation substrates within glycolytic metabolic processes. Two control enzymes of the glycolytic pathway, hexokinase 2 (HK2) and phosphofructokinase muscle form (PFK1), were identified as *bona fide* ISGylation targets during infection. In an integrative approach complemented with enzymatic functional testing and structural modeling, we demonstrate that protein ISGylation obstructs the activity of HK2 and PFK1. Seahorse-based investigation of glycolysis in cardiomyocytes revealed that, by conjugating proteins, the ISG15 system prevents the infection-/IFN-induced upregulation of glycolysis. We complemented our analysis with proteomics-based advanced computational modeling of cardiac energy metabolism. Our calculations revealed an ISG15-dependent preservation of the metabolic capacity in cardiac tissue during CVB3 infection. Functional profiling of mitochondrial respiration in cardiomyocytes and mouse heart tissue by Seahorse technology showed an enhanced oxidative activity in cells with a competent ISG15 system.

Conclusions: Our study demonstrates that ISG15 controls critical nodes in cardiac metabolism. ISG15 reduces the glucose demand, supports higher ATP production capacity in the heart, despite nutrient shortage in infection, and counteracts cardiac atrophy and dysfunction.

Translational perspective

Viral infection imposes a catabolic state with systemic shortage of plasma nutrients, thereby imposing metabolic stress to the heart muscle, which is highly dependent on adequate energy supply. Here, we explored molecular aspects of ISGylation, an endogenous stress-induced protein

modification machinery induced by interferons in cardiac tissue during viral infection. We uncovered that the ISG15 system supports the heart muscle to meet its energetic demand. By conjugating ISG15 to control enzymes of glycolysis, ISG15 lowers the glucose flux under conditions of infection-triggered hypoglycemia. At the same time, ISG15 enhances the respiratory activity in mitochondria, all ensuring the metabolic capacity of the heart during viral infection.

Keywords: metabolism, ISG15, ISGylation, virus infection, glycolysis, mitochondrial function

Abbreviations

AdV	Adenoviral vector
ACoA	acetyl-CoA
ACoAC	ACoA carboxylase
ALDO	fructose-bisphosphate aldolase A
AMPK	AMP-activated protein kinase
BCAA	branched chain amino acids
CPT	palmitoyltransferases
CVB3	Coxsackievirus B3
DTT	dithiothreitol
ECAR	extracellular acidification rate
ENO	β-enolase
FA	fatty acids
FAO	fatty acid oxidation
Frc16BP	fructose-1,6-bisphosphate
Frc6P	fructose-6-phosphate
GAPDH	glyceraldehyde-3-phosphate dehydrogenase
Glc6P	glucose-6-phosphate
GO	gene ontology
GPI	glucose-6-phosphate isomerase
HK2	hexokinase 2
IFN	interferon
IRF	interferon regulatory factor
ISG	IFN-stimulated gene
Iso	isoleucine
LDH	L-lactate dehydrogenase A
Leu	leucine
MTDR	MitoTracker™ Deep Red
OCR	oxygen consumption rate
OXPHOS	oxidative phosphorylation
PER	proton efflux rate
PFK1	phosphofructokinase muscle form
PRR	pattern recognition receptor
PYGM	glycogen phosphorylase muscle form
TCA	tricarboxylic acid

Introduction

Viruses are a common cause of infectious myocarditis, an inflammatory disease of the myocardium that is diagnosed on the basis of histologic, immunologic, and immunohistochemical criteria. Common examples for primary cardiotropic viruses are adenoviruses and enteroviruses. Murine studies with these viruses have identified temporal phases of myocarditis with viral infection of cardiomyocytes, activation of innate immunity and onset of (viral) cytotoxicity, followed by the activation of adaptive immunity with T cell infiltration and potentially autoantibody formation. In most cases, many of these mechanisms support virus clearance and complete resolution of cardiac inflammation [1].

As part of innate immunity aiming to combat infection, host cells, such as cardiomyocytes, possess pattern recognition receptors (PRR) that are activated by viral nucleic acids and promote interferon (IFN) production [2]. There is compelling evidence for the protective function of IFN signaling during viral myocarditis, particularly in the well-established Coxsackievirus B3 (CVB3) infection mouse model [2-4]. After an initial infection of the pancreas and liver, CVB3 infection shows a second wave in mice, which leads to mild and focal injury of the myocardium, with occasional manifestation of chronic heart failure [5-7]. During acute CVB3 infection, IFNs stimulate the expression of ISG15, which is one of the most abundant IFN-stimulated genes (ISGs) in cardiomyocytes [5, 6], imperative for broad-spectrum antimicrobial action[8]. For CVB3 infection, ISG15 acts by covalent modification of lysine residues of target proteins in an E1/E2/E3 (Ube1L, Ube2L6, Herc5/6) enzyme cycle, in a process called ISGylation. During CVB3 infection, the biological activity of protein ISGylation is specifically required in cells of non-hematopoietic origin. Thereby, also cardiomyocytes acquire a protected state which translates into lower virus replication. A stabilization of the pool of ISGylated proteins, accomplished by inactivating the isopeptidase activity of the major de-ISGylating enzyme USP18, suppresses the viral load in heart tissue even further [5].

Undoubtedly, the virus-suppressive activity of ISG15 represents a main aspect how ISG15/ISGylation mitigates inflammatory cardiac tissue damage in mice [5, 6]. Nevertheless, in recent work unrelated to the ISG15 field, we and others demonstrated that systemic pathology with hemodynamic compromise and weight loss during CVB3 infection is, if at all, only marginally attributable to viral cytotoxicity and inflammatory damage responses in heart tissue [9, 10]. CVB3

infection of the heart induces small inflammatory foci, while the vast majority of cardiomyocytes, as well as systolic function of the ventricle, remain intact [9]. Therefore, it remains unclear if and to what extent the virus-suppressive activity of ISG15 attributes to maintained cardiac performance during CVB3 infection of mice.

More recently, a biological role for IFN on energy metabolism came into focus, with yet unknown impact for cardiac metabolism. Cardiomyocytes need to adapt to physiological changes constantly and the heart possesses the ability to use a wide range of different substrates as metabolic fuel [11]. The majority of cardiac ATP originates from the oxidation of long-chain FA (FAO), their supply being ensured by demand-controlled liberation of FA from adipose tissue [12]. Most of the remaining ATP is derived from the oxidative metabolism of glucose [12]. The cellular responses stimulated by IFN signaling involve a higher glucose uptake [13] and stimulated FAO and oxidative phosphorylation (OXPHOS) [14]. Consequently, by PRR and IFN signaling, virus infection can impose metabolic stress on the body that is also found in mice upon CVB3 infection [5]. Nevertheless, it is unclear how cardiac metabolism responds to infection, and whether ISG15/ISGylation influences the crosstalk between the ATP-generating pathways in the heart. Recent data point towards an ISG15-dependent increase of mitochondrial respiration in virus infection [5, 15], and in CVB3 infection, ISG15 shapes the liver proteome towards a temporally enhanced gluconeogenesis capacity [5]. Nevertheless, both the molecular aspects and functional consequences of ISG15/ISGylation on energy production in infection remain unresolved. Therefore, we set up a study to explore the underlying aspects how the ISG15 system controls cardiac homeostasis during CVB3 infection. Therefore, we focused on the protein targets of the ISGylation machinery in heart tissue, questioning the functional implication of this protein modification.

Materials and Methods

Mice

Mice were housed at the Charité University Medical Center animal facilities. C57BL/6 mice were obtained from in-house breeding. $ISG15^{-/-}$, $ISG15^{+/+}$, and $USP18^{C61A/C61A}$. and $Ube1L^{-/-}$ mice have been described elsewhere [16-18]. $USP18^{C61A/C61A}$ and wild-type littermates were bred from $USP18^{C61A/wt}$ x $USP18^{C61A/wt}$ stocks, while $ISG15^{-/-}$ and their wild-type littermates were bred from $ISG15^{-/+}$ x $ISG15^{-/+}$ mice. $USP18^{C61A/C61A}$ and $ISG15^{-/-}$ mice were backcrossed to C57BL/6 for 10 generations. For isolation of primary cardiomyocytes shown in Figure 5C-D, $USP18^{C61A/C61A}$ x $ISG15^{-/-}$ mice were bred accordingly to [5]. For infection, 4-8 week old male mice received an intraperitoneal injection of $1x10^5$ plaque-forming units (pfu) of Coxsackievirus B3 (CVB3) (Nancy, with the exception for Figure 1C: H3). Three (T1) and eight (T2) days after infection, hearts were isolated and processed for experiments. To identify dropouts for the CVB3 infection model (e.g. non-infected mice where infection did not manifest despite injection of CVB3), we visualized cellular injury and inflammation on cross sections of the pancreas that were stained with hematoxylin and eosin. CVB3 infection results in acute virus- and inflammatory tissue destruction of the pancreas. Animals of a lack of this respective injury were classified as non-responder to CVB3 injection and considered as a dropout without further analysis in this study (<10 %). Echocardiography is described in the Supplemental Material. Induction of anesthesia was carried out with 5 % isoflurane and maintained with 1.5-2.5 % isoflurane via mask ventilation. This study was carried out in compliance with the *Guide for the Care and Use of Laboratory Animals* of the German animal welfare act, based on the directive of the European parliament and the council for the protection of animals used for scientific purposes. It follows the Institutional Animal Care and Use Committee guidelines. Protocols were approved by the local authorities for animal welfare in Berlin (permit numbers: G0272/14, G0070/18, G0119/20, G0139/20). Mice were sacrificed in isoflurane anesthesia by increasing the dosage of the anesthetic. All efforts were made to minimize suffering.

Cell culture and adenoviral vectors

The isolation and culture of primary, day-14-embryonic cardiomyocytes, yielding >90% troponin-I-positive cells, has been described elsewhere [20]. We obtained about 7-9 embryos for both WT and $ISG15^{-/-}$ condition from each mother and sacrificed 1-2 animals for each experiment. Cardiomyocytes were infected with CVB3 at an MOI of 1.0 for 6 - 8 hours. Alternatively, cells

were treated with 100 U/ml mouse IFN-β for 24 hours. To distinguish ISG15 function between free and conjugated ISG15, USP18$^{C61A/C61A}$ x ISG15$^{-/-}$ cardiomyocytes were transduced with adenoviral vectors (AdV) expressing murine HA-ISG15-LRGG or unconjugatable murine HA-ISG15-LRAA at MOI 25 for 8 hours, followed by a 16 hour stimulation with IFN-β. AdV particles were generated by the Viral Core Facility of the Charité-Universitätsmedizin Berlin. Briefly, cDNAs from mISG15-LRGG (wild-type) and mISG15-LRAA (unconjugatable ISG15) were cloned into pShuttle-CMV (Addgene plasmid #16403) and used for recombination in pAdEasy1 cells (Addgene plasmid #16399) to generate pAdEasy-CMV-mISG15-LRGG and pAdEasy-CMV-mISG15-LRAA. AdV particles were produced by transfecting linearized, recombinant pAdEasy plasmids (PacI digest) into HEK293A cells. After purification by CsCl ultracentrifugation, viruses were titered in HEK293A cells by serial dilution and anti-hexon immunocytochemistry (ab2596 from Abcam) [21]. HeLa (ATCC) cells were cultured in DMEM supplemented with 10% (v/v) Fetal Calf Serum (FCS) and 1% (v/v) penicillin/streptomycin and ISGylation target gene expression was induced by transfection of expression vectors (Table 1) using polyethylenimine (Polyscience Inc., Warrington, PA, USA). Cells were grown to ~80% confluence and ISG15 and the ISGylation machinery expression was induced by transfection of pcDNA3.1-HA-ISG15, pcDNA3.1-Ube1L, pcDNA3.1-UbcM8, and pTriEx2-HERC5 using polyethylenimine (Polyscience). The empty backbone vector (pcDNA3.1) or pEGFP-C3 were used as control.

Immunoprecipitation

HeLa cells were transfected as described above and lysed in 20 mM HEPES, 8 mM EDTA, 2 mM EGTA, 1% CHAPS, 50 mM sodium fluoride, 5 mM sodium pyrophosphate, 2 mM sodium orthovanadate, 5 mM N-ethylmaleimide (NEM) and cOmplete Protease Inhibitor Cocktail (Roche, Basel, Switzerland). Total protein content was determined by Bradford assay and 1.5 - 2 mg of total protein were subjected to FLAG- and HA-immunoprecipitation using ANTI-FLAG ® M2 Affinity gel (Merck, Darmstadt, Germany), µMACS^{TM} HA Isolation Kit (Milteny Biotec, Bergisch-Gladbach, Germany), Pierce^{TM} Anti-HA Magnetic Beads (Thermo Fisher Scientific, Waltham, MA, USA), or Anti-GFP mAB-Magnetic Beads (MBL Life Science, Tokyo, Japan). For elution, beads were incubated with either Laemmli buffer or 3x FLAG peptide. Samples were analyzed by SDS-polyacrylamide gel electrophoresis (SDS-PAGE).

Site-directed mutagenesis & enzyme activity assays

The identified ISGylation sites of HK2 and PFK1 were subjected to site-directed mutagenesis using the primers depicted in Table 2. Identified K residues were mutated to R, abolishing ISGylation at these sites. Expression and immunoprecipitation of FLAG-tagged hexokinase 2 (HK2) and phosphofructokinase1 (PFK1) in sgISG15 HeLa cells (ISG15-ko cells) [5] was performed as described above. HK2 and PFK were eluted from beads with 3x FLAG peptide prior to activity analysis with the HK Activity Assay Kit (MET-5087, Cell Biolabs Inc., San Diego, CA, USA), or the PFK Activity Assay Kit (PK-CA577-K776, PromoCell GmbH, Heidelberg, Germany), respectively. Activity assays were performed according to the manufacturer's instructions. Enzyme activities in mU/µg were normalized to expression levels determined by Western Blot and calculated relative to the control condition.

Western Blot

SDS-PAGE and Western Blot analysis were performed according to standard protocols. The following primary antibodies were used for protein detection: FLAG (F1804; Sigma-Aldrich, St. Louis, MO, USA), HA (ab9110; Abcam, Cambridge, UK), α-tubulin (GT114; GeneTex, Irvine, CA, USA), GAPDH (sc-25778; Santa Cruz Biotechnology, Inc., Dallas, TX, USA), GFP (PA1-980A; Thermo Fisher Scientific). Secondary IRD680CW- or IRDye800CW-labeled antibodies were detected by an Odyssey CLx infrared imaging system (LI-COR Biosciences, Lincoln, NE, USA). Complete unedited gels for each representative cropped gel within the manuscript and supplemental material are presented in Supplemental Figures S6-S8.

Seahorse metabolic measurement

To determine mitochondrial oxidative metabolism and glycolytic capacity, primary cardiomyocytes and heart biopsies (1mm punches) were analyzed with a Seahorse XFe 96well Extracellular Flux Analyzer (Agilent Technologies, Santa Clara, CA, USA). Further information is provided in the Supplemental information.

Mitochondrial staining with MitoTracker™ Deep Red

Primary cardiomyocytes were stained with 2 nM MitoTracker™ Deep Red (Cell Signaling Technology, Danvers, MA, USA) in growth medium for 30 min at 37°C and subsequently

trypsinized and spun down at 200 rcf for 3 min. Further information is provided in the Supplemental Material.

Proteomic sample preparation & di-glycine (GG)-enrichment

Three mice per genotype and condition (USP18$^{C61A/C61A}$, wild-type, and ISG15$^{-/-}$) were infected as described, monitored, and weighed daily. At the indicated time points, animals were sacrificed and whole hearts were collected and flash-frozen in liquid nitrogen. Tissue work-up was performed according to [22] and is described in the Supplemental Material.

Computational modeling of cardiac metabolic capacities

For computational metabolic modeling, the CARDIOKIN1 platform [29] was employed. CARDIOKIN1 comprises all pathways involved in catabolism of the energy-delivering substrates glucose, lactate, fatty acids, ketone bodies (KBs) and branched-chain amino acids (BCAAs) as well as the synthesis of endogenous energy stores (glycogen, triacylglycerol), taking into account regulation of metabolic enzymes and transporters by substrate affinities, allosteric regulations as well as short-term regulation by the hormones insulin and catecholamines. Model instantiations are based on protein abundances, obtained from individual cardiac proteomic profiles. Cardiac proteomes were generated from the protein discs made available by the Bligh & Dyer extraction for metabolomics, described above. Further information is provided in the described in the Supplemental Material. The protein disks were dissolved in 200 µL lysis buffer containing 7 M urea and 0.1 M

Statistics

Statistical analysis was performed in GraphPad Prism v7.00/8.00/9.00 for Windows (GraphPad Software, San Diego, CA, USA) or Perseus software (version 1.6.2.1, MaxQuant, Martinsried, Germany). Data in GraphPad was plotted as individual points and summaries are given as mean ± SEM unless indicated otherwise. Two group comparisons were analyzed with unpaired *t*-tests. If an *F*-test determined unequal variances, an unpaired *t*-test with the Welch correction was performed. One-sample *t*-tests were used when values were normalized to an internal control. Multiple group comparisons were conducted with unequal variance versions of ANOVA (one-way or two-way) with subsequent multiple comparisons test. Significance threshold was set at 0.05

unless indicated otherwise. MS proteomics data were deposited to the ProteomeXchange Consortium via PRIDE [33] partner repository, receiving the dataset identifier PXD032078.

Results

ISG15 preserves cardiac function and reduces wasting

We endeavored to elucidate the molecular aspects how ISG15 affects the cardiac phenotype during CVB3 infection. We infected ISG15$^{-/-}$ mice and wild-type (WT) controls with CVB3, and after 8 days, measured a reduction of the cardiac output due to ISG15 deletion. The cardiac output was significantly lower in ISG15$^{-/-}$ mice in comparison to infected WT controls (Figure 1A). The systolic function, as exemplified by left ventricular ejection fraction (LVEF), was not substantially altered in infected ISG15$^{-/-}$ mice, indicating that other parameters contribute to cardiac output failure. In fact, we identified lower heart rates and a reduced filling capacity, the latter coinciding with loss of ventricular mass during infection. Infected ISG15$^{-/-}$ mice had reduced left ventricular dimensions and cardiac mass with lower end-diastolic volume (Table Supplement T1, Figure 1A). Notably, during CVB3 infection, we observed a correlation between a drop in cardiac mass with output failure (Figure 1B), suggesting cardiac atrophy as a main parameter for the observed phenotype. Therefore, we investigated how the ISG15 system, which is highly activated as early as at day 3 after CVB3 infection (T1) [5], might affect wasting events. We monitored body and heart muscle mass after 3 (T1) and 8 days (T2). In comparison to WT controls, ISG15$^{-/-}$ mice showed an enhanced reduction in body mass (Figure 1D). More strikingly, a substantial loss of heart mass became evident in infected mice, which was also more pronounced in ISG15$^{-/-}$ mice (Figure 1E). In conclusion, the ISG15 system apparently controls processes that preserve heart muscle integrity and this appears to be a critical aspect for maintenance of cardiac function during infection.

Protein ISGylation targets rate-limiting enzymes of cardiac glycolysis

The overall protective effects mediated by ISG15 rely on the protein modifier function of ISG15, with a strong physiological significance of protein ISGylation during CVB3 infection [5, 6]. Therefore, we sought to identify the protein targets of ISG15 in heart tissue and their respective modification sites to explore the molecular aspects of ISG15 function *in vivo*. We analyzed the cardiac ISGylome using an experimental set-up comparing WT and ISG15$^{-/-}$ mouse hearts at T1 and T2 with uninfected control mice (Figure 2A) [22]. Cardiac peptides were enriched by their Gly-

Gly(GG)-modified sites, representing either ISGylation or ubiquitination, and identified by mass spectrometry. As a positive control, we investigated USP18$^{C61A/C61A}$ mice, where the deISGylation activity of the major ISG15 protease USP18 has been selectively inactivated [34]. Statistical analysis and subsequent non-supervised hierarchical clustering of the identified modification sites revealed distinct clusters of sites (Figure 2B/C, Table Supplement T2). The GG-modification sites present in WT and USP18$^{C61A/C61A}$ mice, but absent in ISG15$^{-/-}$ mice, were assumed to be *bona fide* ISGylation sites. We identified 51 such sites on 37 proteins at T1 (Figure 2B, Table Supplement T2) and 70 ISGylation sites on 41 proteins at T2 (Figure 2C, Table Supplement T2). In line with previous findings [22], based on the amino acids surrounding the identified sites, we did not detect any specific motif (Figure 2D). Some proteins, such as aldolase A, myosin-6/7, and transketolase, were found to be both targets of ISG15 and ubiquitin. Out of all the GG-modification sites at T1 and T2, 30 were identified at both time points of infection. Of these overlapping sites, eight were found in a different cluster at T2, with the majority changing from ISGylation to ubiquitination (Table Supplement T3). The ubiquitylome contained mainly cardiac structural proteins, such as titin and myosin (Table Supplement T2). Comparing previously identified ISG15 targets from cells or other tissues [22, 36-39] to those found in our study, we found 12 novel ISG15 targets, among them the metabolic enzymes phosphofructokinase muscle form (PFK1) and glycogen phosphorylase muscle form (PYGM), and reported 62 novel ISGylation sites (Table Supplement T4).

We next performed a systematic Gene Ontology (GO) search for the cardiac ISGylome. At T1 we found an enrichment for ISGs, such as IFIT1/3 and STAT1, known to be important in regulating the host defense response against CVB3 (Figure 2E, Table Supplement T5). Notably, we uncovered a strong enrichment of ISGylation substrates within metabolic GO terms, namely glycolytic and ATP metabolic processes, both at T1 and T2 (Figure 2E/F, Table Supplement T5/6). In fact, several enzymes of the glycolytic pathway were identified as *bona fide* ISGylation targets during infection, including hexokinase 2 (HK2), glucose-6-phosphate isomerase (GPI), PFK1, fructose-bisphosphate aldolase A (ALDO), glyceraldehyde-3-phosphate dehydrogenase (GAPDH), β-enolase (ENO), L-lactate dehydrogenase A (LDH), with their respective ISGylation sites being depicted in Figure 3A. We verified the ISGylation of these targets in HeLa cells, where the ISGylation machinery (HA-tagged ISG15, the E1 (Ube1L), E2 (Ube2L6), and E3 (Herc5) enzymes) was overexpressed together with the FLAG-tagged glycolysis enzymes which were subsequently immunoprecipitated. First, the experimental set-up was validated with GFP serving

as a negative control [40], as GFP is not modified by ISG15 (Figure Supplement S3, [41]). Pulldown of FLAG-tagged proteins revealed higher molecular weight versions for all of the GG-IP/MS-defined ISGylation targets, confirming ISGylation of the glycolysis enzymes HK2 and PFK1 (Figure 3B/C), as well as ALDO, GAPDH and LDH (Figure Supplement S2). ISGylation of the proteins was independently confirmed by HA-pulldowns of ISGylated proteins (Figure Supplement S1/S2).

The ISG15 system is a negative regulator of glycolysis

The high proportion of ISGylation targets among glycolytic enzymes in cardiac tissue at T1/T2 prompted us to investigate the functional properties of the ISG15 system on glycolysis. In this catabolic carbohydrate pathway, the reactions catalyzed by HK2 and PFK1 serve as the primary control nodes of the pathway, and based on this, we focused on these two substrates for ISGylation. First, we tested whether the ISGylation sites we identified in heart tissue at T1/T2, namely K419 for HK2 and K372 and K727 for PFK1, are unique or whether there might be alternative ISGylation sites. We generated HK2-K419R and PFK1-K327R/K727R mutants and conducted the ISGylation experiments outlined above in HeLa cells. Figure 3 demonstrates a similar ISGylation pattern for both HK2-K419R (Figure 3D) and PFK1-K327R/K727R mutants (Figure 3E), without qualitative differences relative to the wt construct, demonstrating that ISGylation is indeed not restricted to the specific lysine residues that we identified by MS analysis (Figure 3A, Table Supplement T2).

We further questioned whether ISGylation of HK2 and PFK1 has an impact on their substrate turnover rates. Therefore, we explored the effect of this protein modification on the catalytic activity of these rate-limiting glycolytic enzymes. We co-transfected FLAG-tagged HK2 or PFK1 plasmid constructs together with the E1/E2/E3 components into ISG15-ko cells [5] and either restored ISG15 expression or transfected GFP as a control. We then performed immunoprecipitations using FLAG-beads and subjected the enriched enzymes to functional assays (Figure 4A-C). We normalized the catalytic activity of either HK2 or PFK1 to a condition without ISG15 (and ISGylation) as negative control. We found that ISGylation significantly reduced the catalytic activity of both HK2 and PFK1, in comparison to enzymes enriched from cells lacking ISG15. Notably, the HK2-K419R mutant fully restored HK2 activity (Figure 4B), demonstrating that ISGylation of HK2 at K419 indeed reduces Glc6P production. For the PFK1-K327R/K727R mutant, we found, however, a similar reduction in activity by ISGylation as for the wt PFK1 (Figure

4C), indicating that other ISGylation sites are responsible for the observed decrease of PFK1 enzymatic activity in ISGylation-competent cells.

To evaluate a potential impact of identified residues on ISG15 binding at HK2 and PFK1 from a structural perspective, we analyzed known enzyme and ISG15 structures or designed structural models (Figure 4D-H). They imply that indeed K419 in HK2 at the 3-dimensional level is closely located to the substrate binding site (Figure 4D-E), indicating that ISGylation at K419 in a specific mode should prevent substrate binding or enzymatic action, which is in agreement to the experimentally confirmed blocking of Glc6P production by ISGylated HK2 (Figure 4B). In contrast, K327 and K727 in PFK1 are more distant to substrate binding sites (Figure 4G-H), and consequently, ISGylation at these residues would not impede enzymatic activity of the protein as reflected by our experimental data (Figure 4C). However, PFK1 activity is significantly reduced under ISGylation conditions (Figure 5C) and several other positively charged lysine residues are located close to the substrate binding sites (Figure 5G-H). This favors that potential conjugation of ISG15 to one of these alternative Lys-positions would hamper substrate binding or protein activity.

Since we identified ISGylation as a protein modifier of rate control glycolysis enzymes HK2 and PFK1, we next investigated the biological effect of ISG15 on glycolysis in cardiomyocytes, using a specialized Seahorse protocol that tested the glycolytic capacity of WT and $ISG15^{-/-}$ cardiomyocytes during CVB3 infection. While the majority of heart muscle cells during infection *in vivo* represent IFN-activated bystander and not infected cells [2], we also tested how IFN altered the glycolytic activity in cardiomyocytes. Sequential exposure of cells to glucose, rotenone/myxothiazol, and FCCP/monensin (Figure 5A), allowed for the detection of alterations in glycolytic parameters, such as the basal and maximal glycolytic rate as well as the glycolytic rate limited by cellular ATP demand using the Seahorse extracellular flux analyzer [42]. Untreated $ISG15^{-/-}$ cells displayed a slightly higher basal glycolytic level, as reflected by higher proton efflux rate (PER), in comparison to wild-type controls (Figure 5B). This difference became more pronounced once cells were infected or stimulated with IFN. Both the basal and maximal glycolytic activity remained at baseline levels in wild-type cells, whereas the glycolytic rate and thereby produced ATP was elevated in $ISG15^{-/-}$ cells, both during infection and after IFN treatment (Figure 5B). To verify a role of protein ISGylation relating to altered glycolytic activity in IFN-stimulated cardiomyocytes, we transduced cardiomyocytes from $USP18^{C61A/C61A}$ X $ISG15^{-/-}$ mice with AdV

expressing either mISG15-LRGG (wild-type) or an unconjugatable mISG15-LRAA mutant (Figure 5C). AdV transduction of mISG15-LRGG triggered ISGylation and this was increased further upon IFN-β treatment. In contrast, AdV mISG15-LRAA transduced USP18$^{C61A/C61A}$ X ISG15$^{-/-}$ cardiomyocytes lacked ISGylation, but showed robust ISG15 expression. The basal and maximal glycolytic activity in these ISGylation-incompetent, but ISG15-expressing cells was higher in comparison to cells with intact protein ISGylation, both prior to and upon stimulation with IFN-β (Figure 5D). Altogether, our results show suppression of glycolysis by the ISG15 system due to protein ISGylation in IFN-stimulated cardiomyocytes.

The ISG15 system increases the metabolic capacity of the heart

Other than shown for the strong enrichment of glycolysis enzymes among ISGylation targets, there was no indication that ISGylation targets other metabolic pathways. To investigate how the metabolic capacity in the heart as such was affected during CVB3 infection and how ISG15 might regulate it, we considered another possibility for reprogramming of cardiac metabolism beyond the effects documented for ISGylation. Changes in protein abundance of key metabolic proteins could be an additional mechanism for the control of the cardiac metabolic capacity during infection. Therefore, we quantified the cardiac proteome in WT, USP18$^{C61A/C61A}$ and ISG15$^{-/-}$ mice during infection by mass spectrometry (Table Supplement T7). A principal component analysis (Supplementary Figure 4) showed that the infected samples clustered distinctly separate from uninfected ones, irrespective of their genotype and infection time point. To explore whether alterations in protein abundances of metabolic enzymes might alter the ATP production capacity of the heart during infection, we integrated proteomics-based protein levels into a mathematical modeling platform that enables *in silico* calculation of the ATP-generating capacity of the heart, namely the Cardiokin1 platform [29] (Figure 6A). First, based on the cardiac proteome, we calculated the maximal uptake capacity for all plasma nutrients. We found that ISG15 ensured the uptake of free fatty acids (FAs) during infection, while hearts from ISG15$^{-/-}$ mice displayed a reduced FA uptake capacity at T1 (Figure 6B). With the exception of a higher uptake capacity for lactate in ISG15$^{-/-}$ heart tissue at T2, neither ISG15 nor infection influenced the uptake capacity for glucose, ketone bodies or branched chain amino acids (BCAA).

As a next step, we computed the relative contribution of these energy-delivering substrates to total energy expenditure in the heart. We based our simulations on the individual plasma profiles for

glucose, FA, and lactate in WT and ISG15$^{-/-}$ mice at T1/T2 and calculated their proportional contribution to ATP production at baseline and for a high metabolic workload. Our calculation show that FA are the dominant fuel, irrespective of infection status and the ATP demand. With a drop in plasma FAs that was documented at T1/T2 [5], we calculated a relative increase of glucose-fueled and, with increasing ATP demand, some elevation of lactate-fueled energy production (Figure 6C). In comparison to ISG15$^{-/-}$ mice, hearts from WT mice showed a relatively, but non-significant lower glycolytic activity at T2 under maximal load conditions (Figure 6C). Altogether, by integrating individual cardiac proteomes, the Cardiokin1 platform indicated FAs as the dominant energy source for the heart, with ISG15 controlling the uptake of this primary fuel at T1. Furthermore, the computational simulation of cardiac ATP production (Figure 6D) shows that the deletion of ISG15 reduces the overall oxidative capacity in the heart. We computed a lower ATP production rate in mouse hearts from ISG15$^{-/-}$ mice, particularly at T1.

The ISG15 system increases mitochondrial respiration in cardiomyocytes

Our study demonstrated two aspects how ISG15 affects cardiac metabolism. ISG15, most likely by modifying control enzymes, reduces glycolysis rates in cardiomyocytes (Figure 3-5), and alters the cardiac proteome in a way that preserved the metabolic capacity (Figure 6), despite shortage of plasma nutrients during infection. Based on this, we endeavored to elucidate the impact of CVB3 infection on cardiac energy expenditure, as well as a possible influence of ISG15 on metabolic adaptation with functional assays. We infected cardiomyocytes and measured oxygen consumption rates (OCR), a surrogate for the cellular demand for ATP, with a Seahorse XF analyzer (Figure 7A). We used experimental conditions that show no effect of the ISG15 system on viral replication, translating into similar cytotoxicity and ATP demand in both, WT and ISG15$^{-/-}$ cells. Based on the OCR following sequential application of oligomycin, FCCP, and rotenone/antimycin A, we calculated basal and maximal respiration, as well as ATP production (Figure 7B). In comparison to uninfected control samples, infected cells from WT mice displayed a significant increase in basal OCR. Consistently, CVB3 infection elevated the ATP turnover as well as the maximal mitochondrial respiratory capacity, indicating an increased ATP production rate and higher metabolic capacity (Figure 7C). To investigate the role of the ISG15 system in this metabolic adaptation, we compared our findings to cells that we isolated from ISG15$^{-/-}$ mice. A direct comparison of mitochondrial respiration in these cells at baseline conditions revealed an overall non-significant reduction of OCR and ATP turnover. Moreover, in comparison to uninfected

ISG15$^{-/-}$ control samples, infected cells lacking ISG15 failed to increase both their basal and maximal OCR (Figure 7C). These data strongly suggest a biological function of the ISG15 system in reprogramming mitochondrial ATP-generating pathways.

OCR, as determined by the Seahorse XF analyzer, primarily reflects the proton motive force at the inner mitochondrial membrane and thus is directly linked to the mitochondrial membrane potential. We tracked the latter by staining primary cardiomyocytes with MitoTracker Deep Red (MTDR) and visualized its accumulation, attributed to alterations of the mitochondrial membrane potential. A direct comparison of WT and ISG15$^{-/-}$ cardiomyocytes revealed an increased MTDR signal in WT cells (Figure 7D/E). The protective effect of ISG15 on the membrane potential was already apparent in steady state conditions, yet more pronounced during infection. We discovered that the infection-triggered increase of the MTDR accumulation required an operative ISG15 system (Figure 7D/E), complementing the results observed by the Seahorse analysis. The lack of an increase of the mitochondrial potential in ISG15$^{-/-}$ cells, as shown by unaltered MTDR signals upon infection, cannot be attributed to morphologic alterations of the organelles, as an autocorrelation-based image correlation spectroscopy of the MTDR signal revealed no change in mitochondrial sizes for any condition (Figure Supplement S5).

These facts prompted us to profile the relevance of ISG15 for control of the metabolic capacity in heart tissue with a functional assay. We collected heart tissue biopsies from left ventricles of WT and ISG15$^{-/-}$ mice at T1/T2 and compared the basal and maximal OCR to biopsies obtained from T0 mice, using the Seahorse XF analyzer platform. As summarized in Figure 7F/G, we found an increase for both basal and maximal OCR beginning at T1 and maintaining at T2 in WT heart tissue, whereas the oxidative metabolism in ISG15$^{-/-}$ heart tissue showed no alteration in infection. We confirmed that this metabolic reprogramming requires protein ISGylation, since heart tissue from Ube1L$^{-/-}$ mice with depletion of protein ISGylation in infection, showed similar results to ISG15$^{-/-}$ heart tissue and lacked the upregulation of the metabolic capacity found in infected WT mice (Figure 7H). Taken together, this *in vivo* profiling of metabolic function demonstrates, consistent with findings in cardiomyocytes, a biological function of ISG15 in reprograming cardiac metabolism towards increased ATP production capacity during infection. This result supports a higher ATP production rate in infected WT mouse hearts in the absence of concordant regulation of glycolysis.

Discussion

Viral infection imposes a catabolic state on mice with a potentially lethal outcome, as shown for pathogens, such as CVB3 [5], SARS-CoV2 [43] and influenza B virus [44]. In this study, we identified a novel role for the ISG15 system in the preservation of cardiac energy homeostasis during CVB3 infection. We uncovered that ISG15 helps the heart muscle to meet its energetic demand under conditions of infection-triggered nutrient shortage, supporting the continuous supply of the body with oxygenated blood. ISG15 controls critical nodes of the interconnected metabolic network in cardiac muscle cells and beyond, thereby equipping the heart with an enhanced mitochondrial metabolic capacity, increasing ATP production. Protein ISGylation blocked cardiac glycolysis and thereby, it reversed the virus-dictated enhancement of glucose utilization.

CVB3 infection triggers a vast increase in the protein synthesis of antiviral effectors, which imposes a high demand for energy on heart cells [45]. We found this high demand is met by an elevated ATP production rate in heart tissue from WT mice. The enhanced metabolic capacity during infection, despite lower supply of heart tissue's main fuels, FA and glucose [5], was directly dependent on ISG15. Higher oxidative ATP production in infected cardiomyocytes and, more importantly, in cardiac tissue was only observed in the presence of ISG15. An increased ATP production in infected cells might, at least in part, stem from the need for the production of protein building blocks by the virus itself [46]. However, the high mitochondrial respiration rate observed in heart tissue biopsies appears to be more than the small viral foci with a generally low cardiac CVB3 concentration at the T1 phase would impose on the cells for their own needs [5]. Moreover, the upregulation of mitochondrial ATP production in an ISG15-dependent manner occurred despite equal cardiac viral concentrations in WT and ISG15$^{-/-}$ mice [5, 6], thus making it implausible that the increased ATP demand, seen in WT heart tissue, is directly coupled to more virus production. Of note, the augmented metabolic capacity of heart tissue during infection can, at least in part, be attributed to the altered abundances of metabolic proteins, as demonstrated by our calculation of the metabolic capacity using the Cardiokin1-platform [29]. This proteomics-based simulation showed a higher ATP generation capacity by heart muscle tissue during infection, again dependent on the ISG15 system. We determined that this effect is accomplished by conjugation of ISG15 to its target proteins. These data strengthen our conclusion that the virus does not itself impose the demand for

protein synthesis leading to the increase of the cardiac metabolic capacity during infection, but instead reflects the demands of the innate immune system.

Supporting evidence for control of ATP production by ISG15 comes from prior cell culture studies that investigated mitochondrial activity in macrophages [15] and pancreatic cancer stem cells [47]. Similar to the results presented here for cardiomyocytes and in heart tissue, ISG15 enhances the oxidative capacity of these other cell types. There is conflicting data for adipocytes, however, where ISG15 appears to suppress the mitochondrial respiratory capacity. These contrasting results are most likely due to the respective experimental conditions, which precluded adipocytes from fueling their oxidative metabolism by FA. Oxygen consumption, therefore, reflected alterations in aerobic glycolysis [39], which we show to be controlled by ISGylation. In other words, it is unclear how mitochondrial respiration, as such, is controlled by ISG15, particularly under conditions in which acetyl-CoA mainly stems from FAO, as shown here and by others is the case for heart muscle [29, 48]. Further support for the biological requirement of the activated ISG15 system for proper mitochondrial ATP production during viral infection comes from the higher FA uptake and ATP production rate that we calculated for WT heart tissue at T1, in comparison to the ISG15$^{-/-}$ condition. Although not studied in detail, there is some indication that ISGylation might have a direct effect on lipid metabolism. A previous study defined acetyl-CoA carboxylase (ACoAC), the key regulatory enzyme of lipid synthesis, as well as carnitine palmitoyltransferases (CPT), needed for FA transfer across the mitochondrial membrane, as targets of ISG15 in liver tissue [22] and in adipocytes [39]. If and how ISGylation influences either the enzymatic activity of ACoAC and CPT, e.g., as proposed for ISGylation of lactate dehydrogenase [39], or might alter their protein abundance, e.g., as shown for IRF3 [49] and IFIT1/3 [5], is unknown. We also considered control of ATP consumption by the ATPase-inhibitory factor 1 (ATPIF1), which blocks the F_0F_1-ATPase. We and others failed to detect ATPIF1 as a target of the ISGylation cascade[22, 39] and the protein was not detected by shot-gun proteomics in heart tissue, we modelled the energetic stability depending on the activity of F_0F_1-ATPase and the calculated changes of the mitochondrial membrane potential were independent of viral infection and ISG15 expression. Therefore, the F_0F_1-ATPase does not provide the basis for an alternative explanation for our findings.

In fact, for the first time, we demonstrate an ISGylation-dependent increase in metabolic capacity in heart tissue during CVB3 infection. In the context of an increased FA uptake capacity and low

carbohydrate availability, this clearly supports an ISG15-mediated improvement of energy production by enhanced FA metabolism in the heart during the acute phase of CVB3 infection in mice. Another remarkable finding of our infection study is the neutralizing capacity of the ISG15 system on the virus-dictated enhancement of glucose turnover. In the absence of ISG15, the infection-induced upregulation of glycolysis is linked to decreased mitochondrial respiration, indicative of a Warburg effect-like uncoupling of glucose catabolism from its oxidative metabolism. Under conditions of systemic hypoglycemia, such as during CVB3 infection [5], non-oxidative metabolism of glucose might contribute to both less efficient ATP production, as potentially also to higher glucose demand. We propose that protein ISGylation of two key glycolysis control enzymes, HK2 and PFK1, is responsible for a major share of the ISG15-mediated reduction of glycolytic flux. ISGylation of both HK2 and PFK1 effectively reduces their catalytic activity. Our structural models of HK2 and PFK1 suggest ISGylation interferes with the accessibility of the substrates glucose and Frc6P, respectively, to their binding sites. Since these two enzymes are rate limiting in glycolytic fluxes, we propose that ISGylation of these enzymes is key for promoting the metabolic shift towards lower glycolytic rates. This adaptation is potentially augmented by ISGylation of other glycolytic enzymes, as shown here and reported by others [22, 39]. Nonetheless, in the absence of a recognizable, distinct ISGylation motif, the molecular principles that define ISGylation remain unknown.

Overall, the responses attributed to protein ISGylation stimulate higher oxidative metabolism, while reducing the overall turnover of glucose during infection. Together, these data point towards an ISG15-mediated metabolic shift, reducing glucose utilization by heart tissue, while maintaining or increasing FAO-fueled mitochondrial ATP production. Another aspect of lower glucose utilization, accomplished by ISG15-mediated metabolic adaptation, might be less need for endogenous glucose production, an energy-demanding process fueled mainly by amino acids that originate from muscle protein breakdown. Particularly in mice lacking ISG15, we documented signs of enhanced muscle wasting, affecting not only the whole body, but also heart mass loss. Cardiac atrophy, e.g. due to muscle protein breakdown by the ubiquitin proteasome system or autophagy [48], correlates with cardiac output failure in ISG15$^{-/-}$ mice, a surrogate for the high mortality in this group [6]. Altogether, this supports the notion that the metabolic shift triggered by the ISG15 system not only reduces the demand for glucose, but might also lower the need for gluconeogenesis, thus preserving muscle protein integrity.

Taken together, our study demonstrates a novel function for protein ISGylation in the heart. ISG15 reprograms cardiac metabolism under the harsh condition of acute infection-triggered hypoglycemia in mice. With this control of critical nodes in cardiac metabolism, ISG15 reduces the glucose demand in cardiomyocytes and, at the same time, it supports increased ATP production capacity, despite systemic nutrient shortage.

Funding

This work was supported by the Foundation for Experimental Biomedicine Zurich, Switzerland. The Deutsche Forschungsgemeinschaft (DFG, German Research Foundation) supported this project – Project-ID INST 39/1216-1 – CRC/TRR 167 (B16N), Project-ID 318346496 – SFB1292/2 (TP02), Project-ID BE 6335/4-3, BE 6335/5-1 to AB and CRC1470 (A08) to AB and NB. P.S. is supported by the DFG through CRC 1423, project number 421152132, subprojects A01/A05/Z03; through CRC 1365, project number 394046635, subproject A03; through CRC 1078, subproject B06; through Germany's Excellence Strategies − EXC2008/1 (UniSysCat) – 390540038 and through the Einstein Center of Catalysis (EC^2). CB and MK received support by International Max Planck Research School for Infectious Diseases and Immunology (IMPRS-IDI), Berlin. The work of NG was supported by the DFG SFB958/Z02 to JS and the Advanced Medical Bioimaging Core Facility (AMBIO) of the Charité -Universitätsmedizin. FI was supported by Infect-ERA BacVIRISG15 and an Odysseus type 2 grant from the Research Foundation Flanders (G0F8616N). NB was supported by the Bundesministerium für Bildung und Forschung (German Federal Ministry of Education and Research; grant No. 031A427A), under the frame of ERA PerMed, and by the Deutsche Forschungsgemeinschaft (German Research Foundation; project number 422215721). The work of KPK was supported by the DFG Project-ID INST 39/1216-1 – CRC/TRR 167 (B16N) and KN590/7-1.

Acknowledgments

We acknowledge Karolin Voss, Martin Taube, Prisca Kunert, Anika Linder, Marie-Christin Gaerz, and Sandra Bundschuh for excellent technical assistance. The Advanced Medical Bioimaging Core Facility at the Charité supported this project with confocal microscopy. Furthermore, we thank Olena Mackert for establishing the seahorse tissue-biopsy and assay protocol. $Ube1L^{-/-}$ mice were a donation of D.-E. Zhang, as were pcDNA3.1(-)-Ube1L and pcDNA3.1(-)-UbcM8. Lars Ketscher

donated pTriEx2-HERC5. We thank the Charité Core Facility High Throughput Mass Spectrometry and Viral Core Facility for proteomics and AdV production services, Daniela Ludwig for support in sample preparation and Kathrin Textoris-Taube for analytical instrumentation. M. Gotthardt provided the images for the schematic work flows. pShuttle-CMV and pAdEasy1 cells were a gift from Bert Vogelstein.

Author contributions

Conceptualization: A.B. and C.B.; Supervision: A.B., F.I., K.-P.K, P.S., J.K., J.Sp., M.M., and M.R.; Methodology: C.B., F.T., F.I., E.K.W., J.Sch., N.G., A.H., M.M., U.B., M.V., K.R., and N.B. Data acquisition: C.B., F.T., E.K.W., M.K., N.K., U.B.,S.O. and M.M.; Data analysis: C.B., F.T., E.K.W., N.B., M.K., K.K., M.V., N.G., N.K., S.O. and G.K.; Data visualization: A.B., C.B., N.G., G.K., N.K., M.M., and U.B.; Funding acquisition: A.B., F.I., N.B., M.R., and J.Sch. ; Writing ± original draft: A.B., C.B.

Conflict of Interest

JK conducts paid consultancy for Centogene GmbH. All other authors declare no conflict of interest.

Data availability

We have deposited the proteomic data on the PRIDE database under the data set identifier PXD032078. The project name is "Proteomics-based identification of ISG15 modification sites in vivo upon Coxsackie virus infection". The source data underlying all Figures are provided as Source Data file. All other data are available from the corresponding authors upon reasonable request.

Supplemental Material

Supplementary Tables T1 – T8

Supplementary Figures S1 – S5

References

1. Sagar S, Liu PP, Cooper LT, Jr. Myocarditis. *Lancet* 2012;**379**:738-747.
2. Althof N, Harkins S, Kemball CC, Flynn CT, Alirezaei M, Whitton JL. In vivo ablation of type I interferon receptor from cardiomyocytes delays coxsackieviral clearance and accelerates myocardial disease. *J Virol* 2014;**88**:5087-5099.
3. Wessely R, Klingel K, Knowlton KU, Kandolf R. Cardioselective infection with coxsackievirus B3 requires intact type I interferon signaling - Implications for mortality and early viral replication. *Circulation* 2001;**103**:756-761.
4. Koestner W, Spanier J, Klause T, Tegtmeyer PK, Becker J, Herder V, Borst K, Todt D, Lienenklaus S, Gerhauser I, Detje CN, Geffers R, Langereis MA, Vondran FWR, Yuan Q, van Kuppeveld FJM, Ott M, Staeheli P, Steinmann E, Baumgartner W, Wacker F, Kalinke U. Interferon-beta expression and type I interferon receptor signaling of hepatocytes prevent hepatic necrosis and virus dissemination in Coxsackievirus B3-infected mice. *PLoS Pathog* 2018;**14**:e1007235.
5. Kespohl M, Bredow C, Klingel K, Voss M, Paeschke A, Zickler M, Poller W, Kaya Z, Eckstein J, Fechner H, Spranger J, Fahling M, Wirth EK, Radoshevich L, Thery F, Impens F, Berndt N, Knobeloch KP, Beling A. Protein modification with ISG15 blocks coxsackievirus pathology by antiviral and metabolic reprogramming. *Science advances* 2020;**6**:eaay1109.
6. Rahnefeld A, Klingel K, Schuermann A, Diny NL, Althof N, Lindner A, Bleienheuft P, Savvatis K, Respondek D, Opitz E, Ketscher L, Sauter M, Seifert U, Tschope C, Poller W, Knobeloch KP, Voigt A. Ubiquitin-Like Protein ISG15 (Interferon-Stimulated Gene of 15 kDa) in Host Defense Against Heart Failure in a Mouse Model of Virus-Induced Cardiomyopathy. *Circulation* 2014;**130**:1589-1600.
7. Pinkert S, Dieringer B, Klopfleisch R, Savvatis K, Van Linthout S, Pryshliak M, Tschope C, Klingel K, Kurreck J, Beling A, Fechner H. Early Treatment of Coxsackievirus B3-Infected Animals With Soluble Coxsackievirus-Adenovirus Receptor Inhibits Development of Chronic Coxsackievirus B3 Cardiomyopathy. *Circulation Heart failure* 2019;**12**:e005250.
8. Perng YC, Lenschow DJ. ISG15 in antiviral immunity and beyond. *Nature reviews Microbiology* 2018;**16**:423-439.
9. Goetzke CC, Althof N, Neumaier HL, Heuser A, Kaya Z, Kespohl M, Klingel K, Beling A. Mitigated viral myocarditis in A/J mice by the immunoproteasome inhibitor ONX 0914 depends on inhibition of systemic inflammatory responses in CoxsackievirusB3 infection. *Basic Research in Cardiology* 2021;**116**:7.
10. Pinkert S, Kespohl M, Kelm N, Kaya Z, Heuser A, Klingel K, Beling A. Exploration of Analgesia with Tramadol in the Coxsackievirus B3 Myocarditis Mouse Model. *Viruses* 2021;**13**:1222.
11. Doenst T, Nguyen TD, Abel ED. Cardiac metabolism in heart failure: implications beyond ATP production. *Circ Res* 2013;**113**:709-724.
12. Berg JMTJLSL. Biochemistry. Basingstoke: W.H. Freeman, 2012.
13. Burke JD, Platanias LC, Fish EN. Beta interferon regulation of glucose metabolism is PI3K/Akt dependent and important for antiviral activity against coxsackievirus B3. *J Virol* 2014;**88**:3485-3495.
14. Wu D, Sanin DE, Everts B, Chen Q, Qiu J, Buck MD, Patterson A, Smith AM, Chang CH, Liu Z, Artyomov MN, Pearce EL, Cella M, Pearce EJ. Type 1 Interferons Induce Changes in Core Metabolism that Are Critical for Immune Function. *Immunity* 2016;**44**:1325-1336.
15. Baldanta S, Fernandez-Escobar M, Acin-Perez R, Albert M, Camafeita E, Jorge I, Vazquez J, Enriquez JA, Guerra S. ISG15 governs mitochondrial function in macrophages following vaccinia virus infection. *PLoS Pathog* 2017;**13**:e1006651.
16. Ketscher L, Hannss R, Morales DJ, Basters A, Guerra S, Goldmann T, Hausmann A, Prinz M, Naumann R, Pekosz A, Utermohlen O, Lenschow DJ, Knobeloch KP. Selective inactivation of USP18

isopeptidase activity in vivo enhances ISG15 conjugation and viral resistance. *Proc Natl Acad Sci U S A* 2015;**112**:1577-1582.
17. Kim KI, Yan M, Malakhova O, Luo JK, Shen MF, Zou W, de la Torre JC, Zhang DE. Ube1L and protein ISGylation are not essential for alpha/beta interferon signaling. *Mol Cell Biol* 2006;**26**:472-479.
18. Osiak A, Utermohlen O, Niendorf S, Horak I, Knobeloch KP. ISG15, an interferon-stimulated ubiquitin-like protein, is not essential for STAT1 signaling and responses against vesicular stomatitis and lymphocytic choriomeningitis virus. *Mol Cell Biol* 2005;**25**:6338-6345.
19. Zacchigna S, Paldino A, Falcao-Pires I, Daskalopoulos EP, Dal Ferro M, Vodret S, Lesizza P, Cannata A, Miranda-Silva D, Lourenco AP, Pinamonti B, Sinagra G, Weinberger F, Eschenhagen T, Carrier L, Kehat I, Tocchetti CG, Russo M, Ghigo A, Cimino J, Hirsch E, Dawson D, Ciccarelli M, Oliveti M, Linke WA, Cuijpers I, Heymans S, Hamdani N, de Boer M, Duncker DJ, Kuster D, van der Velden J, Beauloye C, Bertrand L, Mayr M, Giacca M, Leuschner F, Backs J, Thum T. Towards standardization of echocardiography for the evaluation of left ventricular function in adult rodents: a position paper of the ESC Working Group on Myocardial Function. *Cardiovasc Res* 2021;**117**:43-59.
20. Opitz E, Koch A, Klingel K, Schmidt F, Prokop S, Rahnefeld A, Sauter M, Heppner FL, Volker U, Kandolf R, Kuckelkorn U, Stangl K, Kruger E, Kloetzel PM, Voigt A. Impairment of immunoproteasome function by beta5i/LMP7 subunit deficiency results in severe enterovirus myocarditis. *PLoS pathogens* 2011;**7**:e1002233.
21. He TC, Zhou S, da Costa LT, Yu J, Kinzler KW, Vogelstein B. A simplified system for generating recombinant adenoviruses. *Proceedings of the National Academy of Sciences of the United States of America* 1998;**95**:2509-2514.
22. Zhang Y, Thery F, Wu NC, Luhmann EK, Dussurget O, Foecke M, Bredow C, Jimenez-Fernandez D, Leandro K, Beling A, Knobeloch KP, Impens F, Cossart P, Radoshevich L. The in vivo ISGylome links ISG15 to metabolic pathways and autophagy upon Listeria monocytogenes infection. *Nat Commun* 2019;**10**:5383.
23. Tyanova S, Temu T, Cox J. The MaxQuant computational platform for mass spectrometry-based shotgun proteomics. *Nat Protoc* 2016;**11**:2301-2319.
24. Tyanova S, Temu T, Sinitcyn P, Carlson A, Hein MY, Geiger T, Mann M, Cox J. The Perseus computational platform for comprehensive analysis of (prote)omics data. *Nat Methods* 2016;**13**:731-740.
25. Ashburner M, Ball CA, Blake JA, Botstein D, Butler H, Cherry JM, Davis AP, Dolinski K, Dwight SS, Eppig JT, Harris MA, Hill DP, Issel-Tarver L, Kasarskis A, Lewis S, Matese JC, Richardson JE, Ringwald M, Rubin GM, Sherlock G. Gene ontology: tool for the unification of biology. The Gene Ontology Consortium. *Nat Genet* 2000;**25**:25-29.
26. The Gene Ontology C. Expansion of the Gene Ontology knowledgebase and resources. *Nucleic Acids Res* 2017;**45**:D331-D338.
27. Mi H, Muruganujan A, Ebert D, Huang X, Thomas PD. PANTHER version 14: more genomes, a new PANTHER GO-slim and improvements in enrichment analysis tools. *Nucleic Acids Res* 2019;**47**:D419-D426.
28. Colaert N, Helsens K, Martens L, Vandekerckhove J, Gevaert K. Improved visualization of protein consensus sequences by iceLogo. *Nat Methods* 2009;**6**:786-787.
29. Berndt N, Eckstein J, Wallach I, Nordmeyer S, Kelm M, Kirchner M, Goubergrits L, Schafstedde M, Hennemuth A, Kraus M, Grune T, Mertins P, Kuehne T, Holzhütter HG. CARDIOKIN1: Computational Assessment of Myocardial Metabolic Capability in Healthy Controls and Patients With Valve Diseases. *Circulation* 2021;**144**:1926-1939.
30. Messner CB, Demichev V, Wendisch D, Michalick L, White M, Freiwald A, Textoris-Taube K, Vernardis SI, Egger AS, Kreidl M, Ludwig D, Kilian C, Agostini F, Zelezniak A, Thibeault C, Pfeiffer M, Hippenstiel S, Hocke A, von Kalle C, Campbell A, Hayward C, Porteous DJ, Marioni RE, Langenberg C, Lilley KS, Kuebler WM, Mulleder M, Drosten C, Suttorp N, Witzenrath M, Kurth F, Sander LE,

Ralser M. Ultra-High-Throughput Clinical Proteomics Reveals Classifiers of COVID-19 Infection. *Cell Syst* 2020;**11**:11-24 e14.
31. Demichev V, Messner CB, Vernardis SI, Lilley KS, Ralser M. DIA-NN: neural networks and interference correction enable deep proteome coverage in high throughput. *Nat Methods* 2020;**17**:41-44.
32. UniProt C. UniProt: the universal protein knowledgebase in 2021. *Nucleic Acids Res* 2021;**49**:D480-D489.
33. Perez-Riverol Y, Csordas A, Bai J, Bernal-Llinares M, Hewapathirana S, Kundu DJ, Inuganti A, Griss J, Mayer G, Eisenacher M, Perez E, Uszkoreit J, Pfeuffer J, Sachsenberg T, Yilmaz S, Tiwary S, Cox J, Audain E, Walzer M, Jarnuczak AF, Ternent T, Brazma A, Vizcaino JA. The PRIDE database and related tools and resources in 2019: improving support for quantification data. *Nucleic Acids Res* 2019;**47**:D442-D450.
34. Ketscher L, Hannss R, Morales DJ, Basters A, Guerra S, Goldmann T, Hausmann A, Prinz M, Naumann R, Pekosz A, Utermohlen O, Lenschow DJ, Knobeloch KP. Selective inactivation of USP18 isopeptidase activity in vivo enhances ISG15 conjugation and viral resistance. *Proceedings of the National Academy of Sciences of the United States of America* 2015.
35. Thery F, Eggermont D, Impens F. Proteomics Mapping of the ISGylation Landscape in Innate Immunity. *Frontiers in immunology* 2021;**12**:720765.
36. Giannakopoulos NV, Arutyunova E, Lai C, Lenschow DJ, Haas AL, Virgin HW. ISG15 Arg151 and the ISG15-Conjugating Enzyme UbE1L Are Important for Innate Immune Control of Sindbis Virus. *J Virol* 2009;**83**:1602-1610.
37. Zhao C, Denison C, Huibregtse JM, Gygi S, Krug RM. Human ISG15 conjugation targets both IFN-induced and constitutively expressed proteins functioning in diverse cellular pathways. *Proceedings of the National Academy of Sciences of the United States of America* 2005;**102**:10200-10205.
38. Radoshevich L, Impens F, Ribet D, Quereda JJ, Nam Tham T, Nahori MA, Bierne H, Dussurget O, Pizarro-Cerda J, Knobeloch KP, Cossart P. ISG15 counteracts Listeria monocytogenes infection. *eLife* 2015;**4**.
39. Yan S, Kumari M, Xiao H, Jacobs C, Kochumon S, Jedrychowski M, Chouchani E, Ahmad R, Rosen ED. IRF3 reduces adipose thermogenesis via ISG15-mediated reprogramming of glycolysis. *J Clin Invest* 2021.
40. Durfee LA, Lyon N, Seo K, Huibregtse JM. The ISG15 Conjugation System Broadly Targets Newly Synthesized Proteins: Implications for the Antiviral Function of ISG15. *Mol Cell* 2010;**38**:722-732.
41. Durfee LA, Lyon N, Seo K, Huibregtse JM. The ISG15 conjugation system broadly targets newly synthesized proteins: implications for the antiviral function of ISG15. *Molecular cell* 2010;**38**:722-732.
42. Mookerjee SA, Brand MD. Measurement and Analysis of Extracellular Acid Production to Determine Glycolytic Rate. *Journal of visualized experiments : JoVE* 2015:e53464.
43. Sun SH, Chen Q, Gu HJ, Yang G, Wang YX, Huang XY, Liu SS, Zhang NN, Li XF, Xiong R, Guo Y, Deng YQ, Huang WJ, Liu Q, Liu QM, Shen YL, Zhou Y, Yang X, Zhao TY, Fan CF, Zhou YS, Qin CF, Wang YC. A Mouse Model of SARS-CoV-2 Infection and Pathogenesis. *Cell host & microbe* 2020;**28**:124-133.e124.
44. Lenschow DJ, Lai C, Frias-Staheli N, Giannakopoulos NV, Lutz A, Wolff T, Osiak A, Levine B, Schmidt RE, Garcia-Sastre A, Leib DA, Pekosz A, Knobeloch KP, Horak I, Virgin HW. IFN-stimulated gene 15 functions as a critical antiviral molecule against influenza, herpes, and Sindbis viruses. *Proceedings of the National Academy of Sciences of the United States of America* 2007;**104**:1371-1376.
45. O'Neill LA, Pearce EJ. Immunometabolism governs dendritic cell and macrophage function. *J Exp Med* 2016;**213**:15-23.

46. Eagle H, Habel K. The nutritional requirements for the propagation of poliomyelitis virus by the HeLa cell. *J Exp Med* 1956;**104**:271-287.
47. Alcalá S, Sancho P, Martinelli P, Navarro D, Pedrero C, Martín-Hijano L, Valle S, Earl J, Rodríguez-Serrano M, Ruiz-Cañas L, Rojas K, Carrato A, García-Bermejo L, Fernández-Moreno M, Hermann PC, Sainz B, Jr. ISG15 and ISGylation is required for pancreatic cancer stem cell mitophagy and metabolic plasticity. *Nature communications* 2020;**11**:2682.
48. Murashige D, Jang C, Neinast M, Edwards JJ, Cowan A, Hyman MC, Rabinowitz JD, Frankel DS, Arany Z. Comprehensive quantification of fuel use by the failing and nonfailing human heart. *Science* 2020;**370**:364-368.
49. Shi HX, Yang K, Liu X, Liu XY, Wei B, Shan YF, Zhu LH, Wang C. Positive regulation of interferon regulatory factor 3 activation by Herc5 via ISG15 modification. *Mol Cell Biol* 2010;**30**:2424-2436.
50. Lin H, Zeng J, Xie R, Schulz MJ, Tedesco R, Qu J, Erhard KF, Mack JF, Raha K, Rendina AR, Szewczuk LM, Kratz PM, Jurewicz AJ, Cecconie T, Martens S, McDevitt PJ, Martin JD, Chen SB, Jiang Y, Nickels L, Schwartz BJ, Smallwood A, Zhao B, Campobasso N, Qian Y, Briand J, Rominger CM, Oleykowski C, Hardwicke MA, Luengo JI. Discovery of a Novel 2,6-Disubstituted Glucosamine Series of Potent and Selective Hexokinase 2 Inhibitors. *ACS Med Chem Lett* 2016;**7**:217-222.
51. Narasimhan J, Wang M, Fu Z, Klein JM, Haas AL, Kim JJ. Crystal structure of the interferon-induced ubiquitin-like protein ISG15. *J Biol Chem* 2005;**280**:27356-27365.
52. Daczkowski CM, Goodwin OY, Dzimianski JV, Farhat JJ, Pegan SD. Structurally Guided Removal of DeISGylase Biochemical Activity from Papain-Like Protease Originating from Middle East Respiratory Syndrome Coronavirus. *J Virol* 2017;**91**.
53. Tian T, Wang C, Wu M, Zhang X, Zang J. Structural Insights into the Regulation of Staphylococcus aureus Phosphofructokinase by Tetramer-Dimer Conversion. *Biochemistry* 2018;**57**:4252-4262.

Tables

Table 1: List of plasmid sources for ISGylation targets.

Gene	Protein Name	NCBI Ref Seq	Vector	Tag	Source
Aldoa	Aldolase A (ALDO)	NM_007438.4	pCMV3	C-terminal FLAG	Sinobiological, Beijing, China
Gapdh	Glyceraldehyde-3-phosphate dehydrogenase (GAPDH)	NM_008084.1	pCMV6	C-terminal FLAG	OriGene, Rockville, MD, USA
Hk2	Hexokinase 2 (HK2)	NM_013820.3	pCMV6	C-terminal FLAG	OriGene, Rockville, MD, USA
Ldha	Lactate dehydrogenase A (LDH)	NM_010699.2	pCMV3	C-terminal FLAG	Sinobiological, Beijing, China
Pfkm	Phosphofructokinase muscle form (PFK1)	NM_001163487.1	pCMV3	C-terminal FLAG	Sinobiological, Beijing, China

Table 2: Primer list for K to R mutagenesis of HK2 K419 and PFK1 K373 and K727.

Gene	ISGylation site	Mutagenesis primer	Orientation
Hk2	K419	GCTCTGTCTACAAGAGACATCCCCATTTTGC	Forward
		GCAAAATGGGGATGTCTCTTGTAGACAGAGC	Reverse
Pfk1	K372	GATGAAGCCATTAGGCTGAGAGGCCGGAGC	Forward
		GCTCCGGCCTCTCAGCCTAATGGCTTCATC	Reverse
	K727	CAGTAACTGAGCTGAGGGACCAGACAGAC	Forward
		GTCTGTCTGGTCCCTCAGCTCAGTTACTG	Reverse

Figures

Figure 1: Cardiac output failure and atrophy during CVB3 infection.
(A) CVB3-infected WT and ISG15$^{-/-}$ mice were subjected to echocardiographic analysis. **(A)** Cardiac output [ml/min] and end-diastolic volume [µL] calculated for hearts from WT and ISG15$^{-/-}$ mice at T0 (baseline) and T2 (8 days after infection). Statistical analysis was performed with a two-way ANOVA and Sidak's multiple comparisons test. Correlation of cardiac output **(B)** and **(C)** calculated left ventricular (LV) mass with end-diastolic volume. Data generated from n=24 WT mice at T0 and T1 (3 days after infection) of CVB3 infection. **(D)** Body and **(E)** heart weight of wild-type and ISG15$^{-/-}$ mice at T1 and T2 of CVB3 infection, normalized to uninfected controls. Significance was determined using two-way ANOVA with Tukey's multiple comparisons test.

Figure 2: Identification of the cardiac ISGylome during CVB3 infection.
(A) The ISGylome and ubiquitylome in heart tissue of CVB3-infected wild-type (WT), USP18$^{C61A/C61A}$, and ISG15$^{-/-}$ mice were analyzed by LC-MS/MS at T0, T1, and T2 (n=3 each). **(B – C)** Heatmap showing non-supervised hierarchical clustering of significantly regulated di-Gly(K) sites at T1 vs. T0 (A) and T2 vs. T0 (B). The number of sites per cluster is indicated in brackets. On the right, the same heatmap is shown with missing values depicted in gray. **(D)** Sequence logos of ISGylated K residues and their 5 surrounding amino acids at T1 and T2 were drawn with iceLogo. **(E)** Gene Ontology enrichment analyses of ISGylated proteins at T1 and T2 was performed. Selected terms are displayed according to their fold enrichment, red meaning high and yellow low enrichment.

Figure 3: Glycolytic control enzymes are targets of ISGylation.
(A) Schematic representation of glycolysis depicting identified ISGylated enzymes and modification sites within CVB3-infected mouse hearts. **(B+C)** Validation of ISG15-modification of hexokinase-2 (HK2) and phosphofructokinase (PFK). HeLa cells were transfected with a four-plasmid combination (HA-ISG15, Ube1L, Ube2L6, Herc5) and FLAG-tagged HK2 **(B)** or PFK **(C)**. FLAG-immunoprecipitation was performed prior to Western blot analysis. Arrows point towards enriched target and modification sites, as indicated. **(D+E)** R mutants of HK2 ISGylation site K419 **(D)** and PFK ISGylation sites K372/K727 **(E)** were generated. Transfection and immunoprecipitation were performed as described in (B+C). ISGylation patterns of HK2 K419R

(D) and PFK K372R/K727R **(E)** were compared by Western blotting. Targets and modification bands are indicated by arrows and brackets.

Figure 4: Impact of ISG15/ISGylation on HK2 and PFK1 activity.
(A–C) ISG15-deficient HeLa cells were transfected with a four-plasmid combination (HA-ISG15 or GFP, together with Ube1L, Ube2L6, and Herc5) and FLAG-tagged HK2 (B) or PFK1 (C) or their respective K to R site mutants. HK2 and PFK1 were enriched by FLAG-immunoprecipitation prior to enzyme activity measurement of HK2 (n=4) and PFK1 (n=3). Measurements [mU/µg] were normalized to baseline activity. Statistical comparisons were achieved by one-tailed and two-tailed *t*-tests. **(D-E)** Lysine 419 is located close to the substrate (Glc6P) binding site in HK2 (surface representation), as revealed by an already determined enzyme structure (PDB ID 5hg1 [50]). Consequently, ISG15 (cartoon representation, PDB 1z2m [51]) bound to K419 with its C-terminal domain would cover this substrate binding site. The provided visualization is not a complex model between HK2 and ISG15, rather a putative orientation is implied. Computational docking of ISG15 to K419 is not feasible using known template structures, since HK2 is always in a substrate bound conformation, while ISG15 would likely bind to an unbound (apo-) HK2 conformation, which can be drastically different. Such structural template is not available; therefore, this scheme is an approximation. However, specific ISG15-bound protease structures (PDB: 5w8u [52]). **(F)** shows that ISG15 can be bound into a cleft-like structure arrangement of the target protein, as would be the case supposed here for the HK2-ISG15 assembling at K419. **(G)** A similar observation can be made at a structural PFK1 model (surface representation, two subunits (orange, beige)) with bound ligands (e.g., Frc6P) where several lysine residues are located close to the ligand-binding sites (red). ISG15 fused with the C-terminal domain to one of these lysine residues would hamper substrate binding, whereby two ISG15 molecules should be bound into cleft-like structural arrangements in a spatial fit-in manner. The visualization again does not show a computational fully fused and modelled ISG15-PFK1 complex, but is a by-hand oriented approximation due to a missing enzyme template structure in a non-substrated state. Therefore, the structural PFK1 conformation accessible for ISG15 is unknown (as for HK2) and cannot be simulated without further information. **(H)** The lysine residues K372 and K727 identified in this study as ISGylation sites were experimentally excluded to have a functional impact on PFK1 activity and are indeed more distantly located to the substrate binding regions. Note: The visualized PFK1 protein model is derived from a phosphofructokinase structure of *Staphylococcus aureus* (PDB 5xz8 [53]). The

sequence of the protein was substituted by mouse PFK1 amino acid sequence for homology (sequence similarity ~83%, BLOSUM 62 matrix). Model representations were created using the PyMol Molecular Graphics System Version 1.3 (Schrödinger, LLC, New York, NY).

Figure 5: Impact of ISG15/ISGylation on glycolysis during CVB3 infection.
(A) Measurement of glycolytic rate in primary cardiomyocytes. Wild-type (WT) and ISG15$^{-/-}$ cells were cultured in low glucose medium and infected with CVB3 or treated with IFN-β prior to Seahorse glycolytic measurement. Injection of glucose induced an increase in glycolysis. Inhibition of the respiratory chain complex I (rotenone) and III (myxothiazol) turns glycolysis into the sole ATP production pathway. FCCP injection breaks down the mitochondrial proton gradient and monensin increases ATP hydrolysis by activating Na^+/K^+ ATPases, resulting in maximal glycolytic rates. **(B)** Proton efflux rates were set relative to WT control and basal, maximal and ATP demand-limited rate were calculated. **(C)** USP18$^{C61A/C61A}$ x ISG15$^{-/-}$ cells were cultured in low glucose medium and ISG15 expression was rescued by AdV transduction of ISG15-LRGG (wt) or HA-ISG15-LRAA (both MOI 25, 8 hours). ISG15 and ISGylation was visualized upon IFN-β stimulation via western blot using antibodies against HA and tubulin as loading control. **(D)** Measurement of glycolytic rate by Seahorse measurement as shown in (A) upon injection of glucose. Proton efflux rates reflecting basal and maximal glycolytic activity were calculated. Data from a representative experiment out of n=3 independent experiments, with 7-9 technical replicates each. **(B)/(D)** Statistical significance was computed by two-way ANOVA, followed by Sidak's multiple comparisons test.

Figure 6: Computational modeling of cardiac metabolism.
(A) Cardiac proteomes of CVB3-infected wild-type (WT) and ISG15$^{-/-}$ mice were used for computational analysis using the metabolic model Cardiokin1 [29]. **(B)** Maximal uptake capacities for fatty acids (blue), glucose (red), lactate (grey), ketone bodies (bd) (purple), and branched chain amino acids (BCAA) (yellow) were defined by the magnitude of flux changes in response to changes in the concentration of corresponding plasma metabolite. **(C)** Computed contribution of the energy-delivering substrates to total energy expenditure at resting and maximal energy demand for T0/T1/T2 conditions, calculated for the experimentally obtained plasma levels for fatty acids, glucose and lactate [5] ($ mean value baseline; § mean value during CVB3 infection). **(D)** Maximal

total ATP production capacity was calculated and normalized to heart mass [µmol/h]. Significance was determined with two-way ANOVA followed by Sidak‘s multiple comparisons test.

Figure 7: Mitochondrial function of cardiomyocytes during CVB3 infection.
(A-C) Primary cardiomyocytes from WT and ISG15$^{-/-}$ mice were infected with CVB3 at an MOI 1.0 for 6-8h. **(B–C)** Seahorse analysis of mitochondrial oxygen consumption rate (representative of n=5 independent experiments). **(B)** Oligomycin inhibits the respiratory chain ATP synthase thus reducing oxygen usage, while FCCP decouples the other complexes, resulting in maximal activity and, hence oxygen consumption. Rotenone and antimycin A inhibit complex I and III of the respiratory chain, respectively, thereby halting cellular oxygen consumption by oxidative phosphorylation. **(C)** Basal respiration, ATP production, and maximal respiration are depicted and were calculated relative to wild-type untreated control cells. Significances were determined using two-way ANOVA with Sidak‘s multiple comparisons test. **(D–E)** MitoTracker Deep Red^{TM} (MTDR) live cell staining in cardiomyocytes to analyze mitochondrial integrity. FCCP pre-treatment for 4 h served as a control. Cells were analyzed by confocal microscopy. Maximum intensity Z-projection is displayed with staining of MTDR in red and DAPI in blue. Scale bar: 10 µm. Quantitative comparison of intensity distributions of MTDR fluorescence (n=24) **(D)**. Flow cytometry analysis of MTDR mean fluorescence intensity, set relative to WT control **(E)**. Statistical analysis was performed by two-way ANOVA followed by Sidak‘s multiple comparisons test. **(F-G)** Mitochondrial function of heart tissue during CVB3 infection. Heart tissue biopsies obtained from wild-type (WT), and ISG15$^{-/-}$ mice at T0, T1, and T2 were analyzed by Seahorse measurement, determining oxygen consumption rates that were normalized to uninfected controls. **(F)** Basal and **(G)** maximal respiration are displayed. *P*-values were determined by Student‘s *t*-test. **(H)** To distinguish between effects of free ISG15 and ISGylation, Ube1L$^{-/-}$ mice were infected and cardiac biopsies were analyzed as described above.

Figure 1

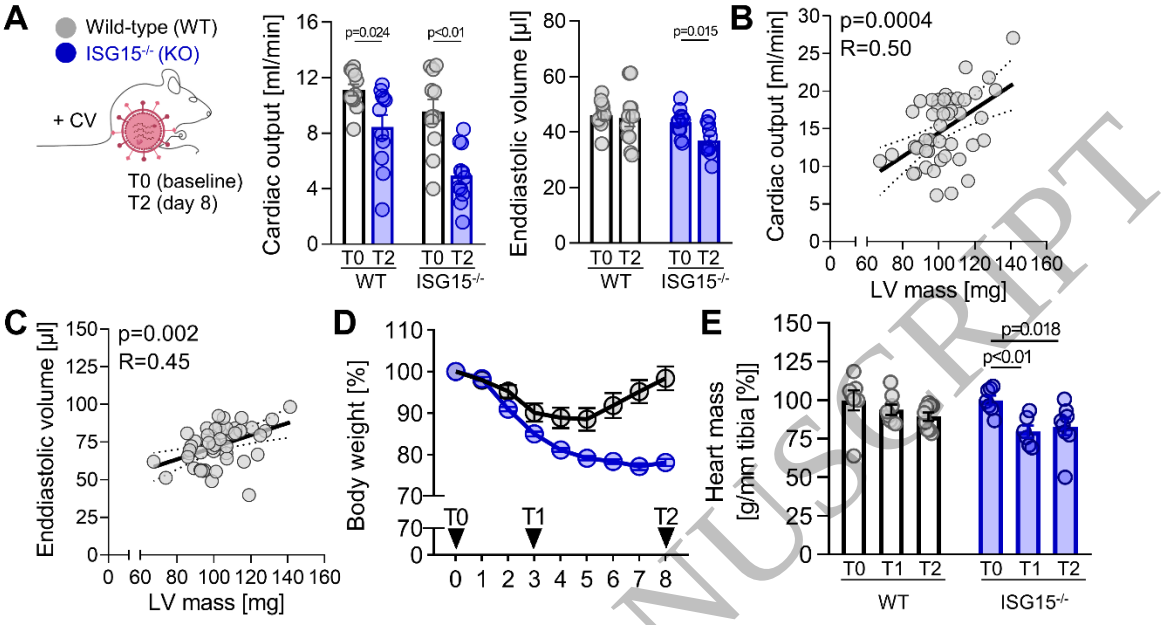

1

2

Figure 2

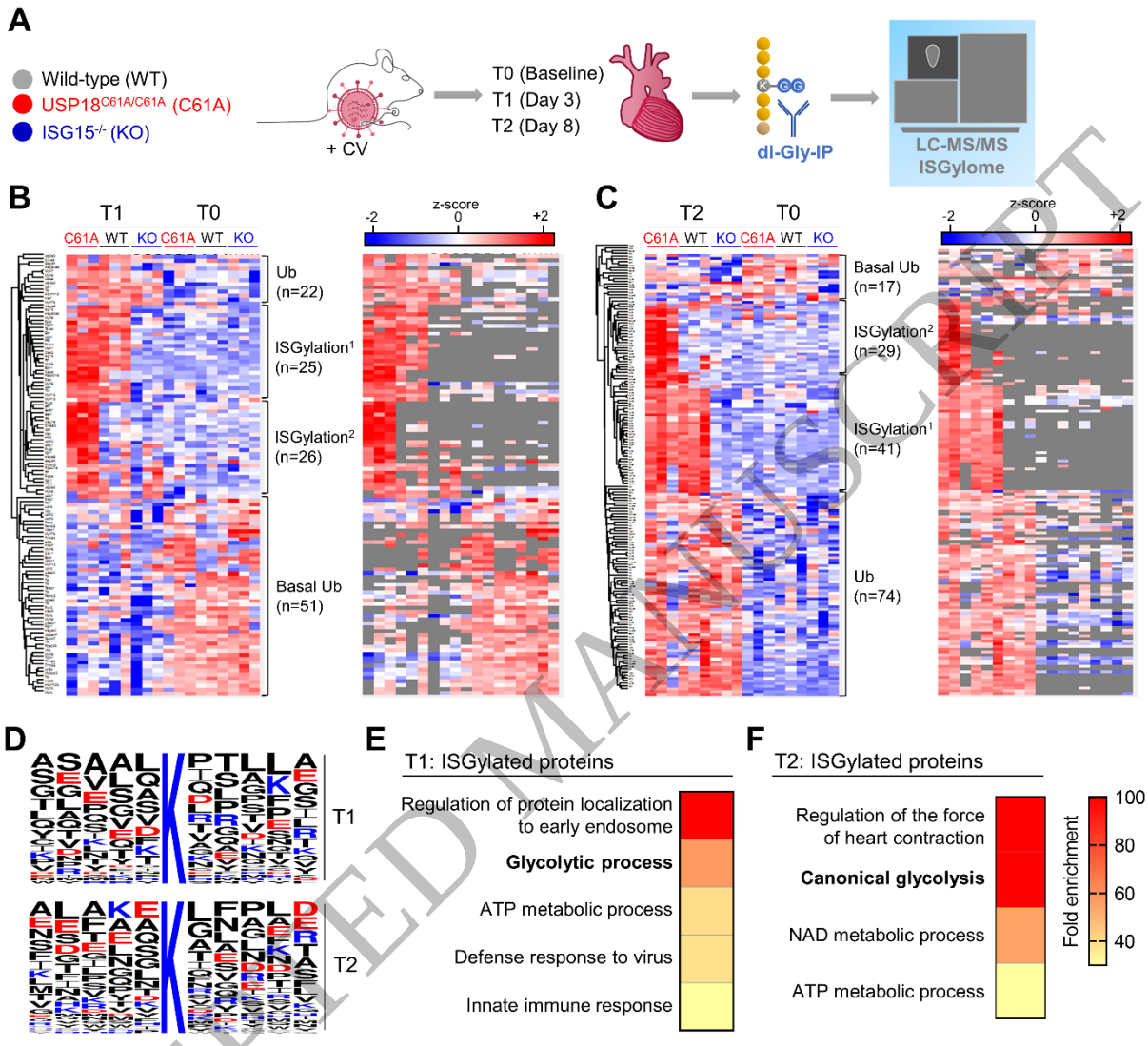

1

2

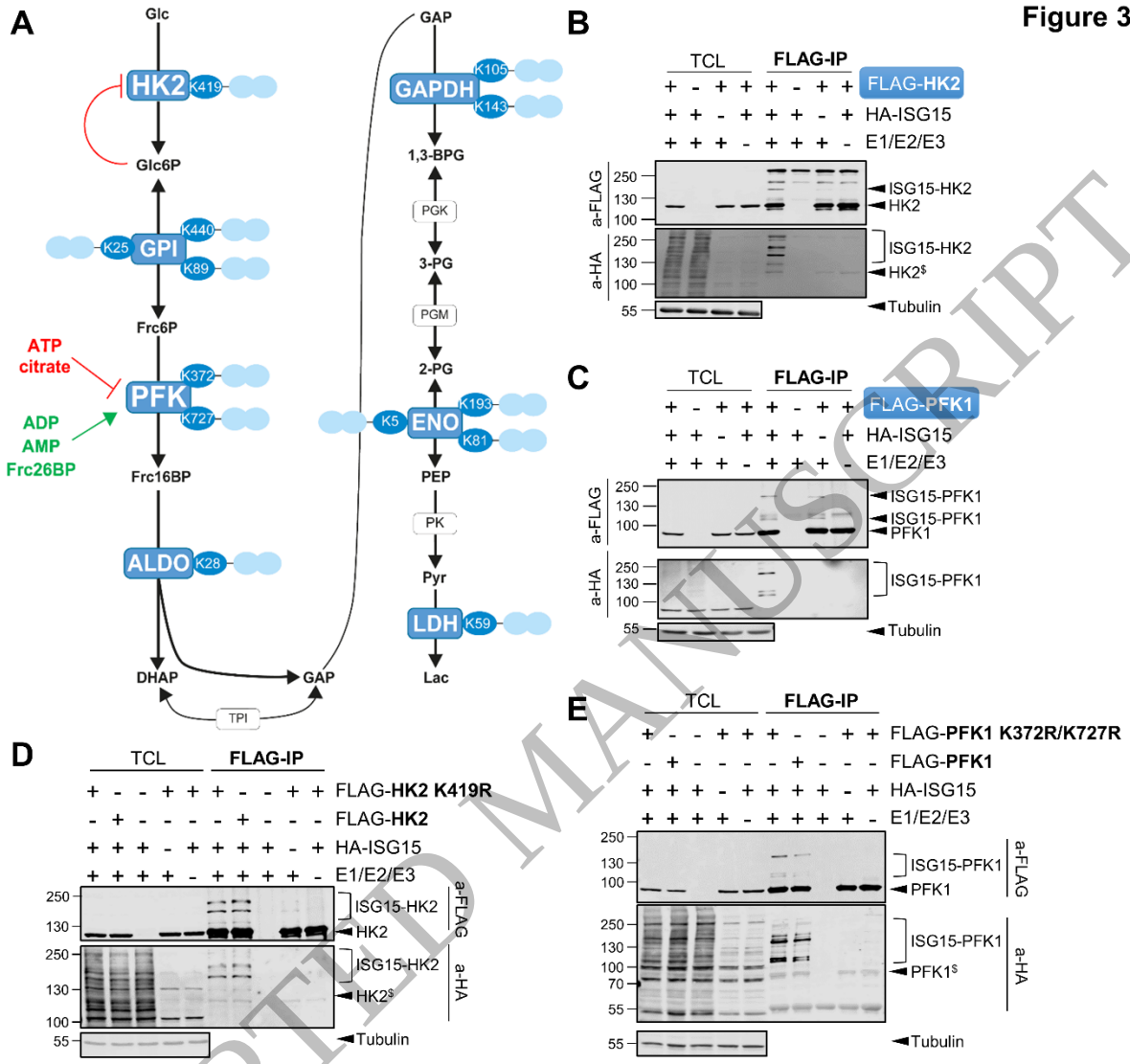

Figure 4

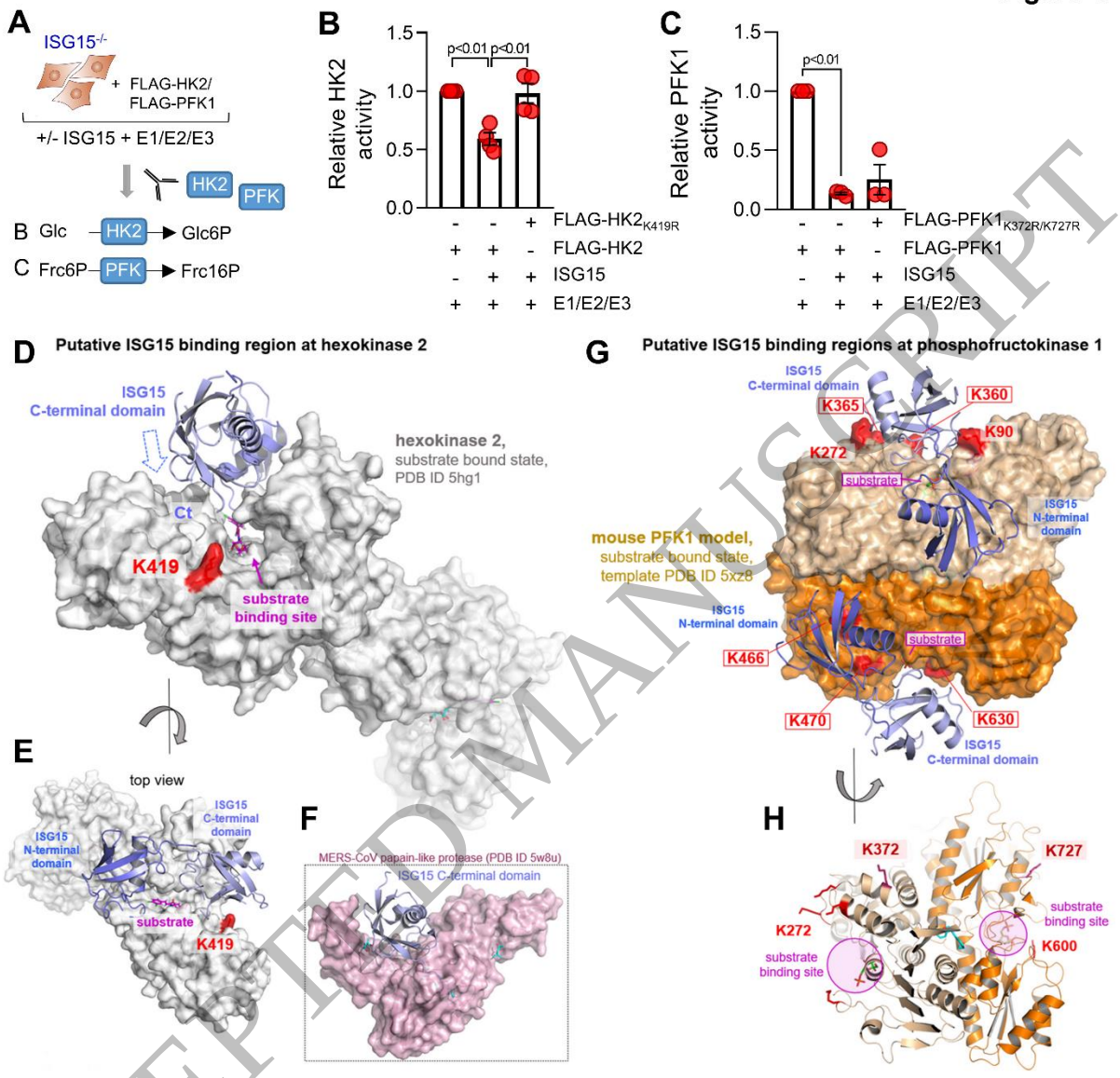

1

2

Figure 5

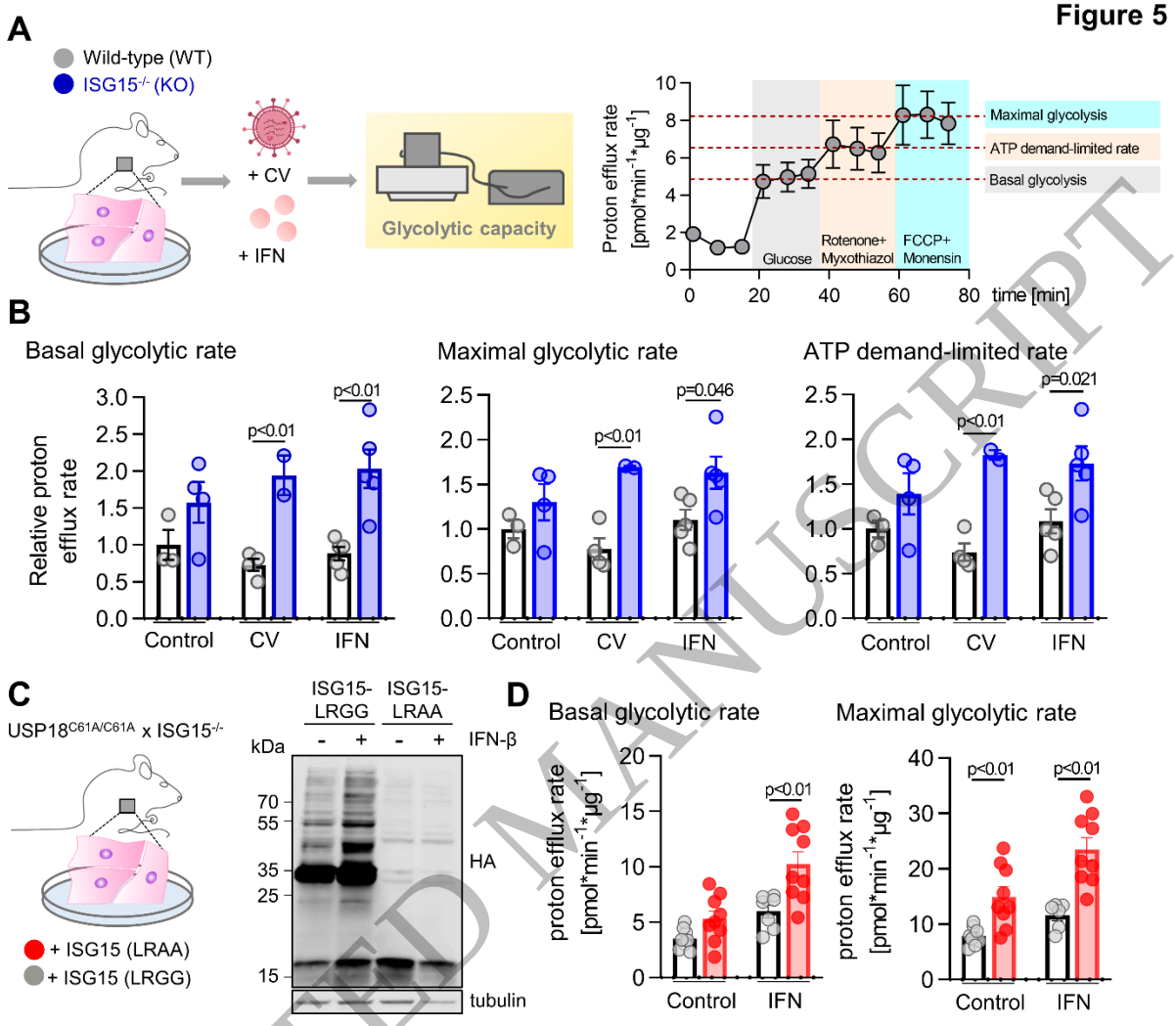

Figure 6

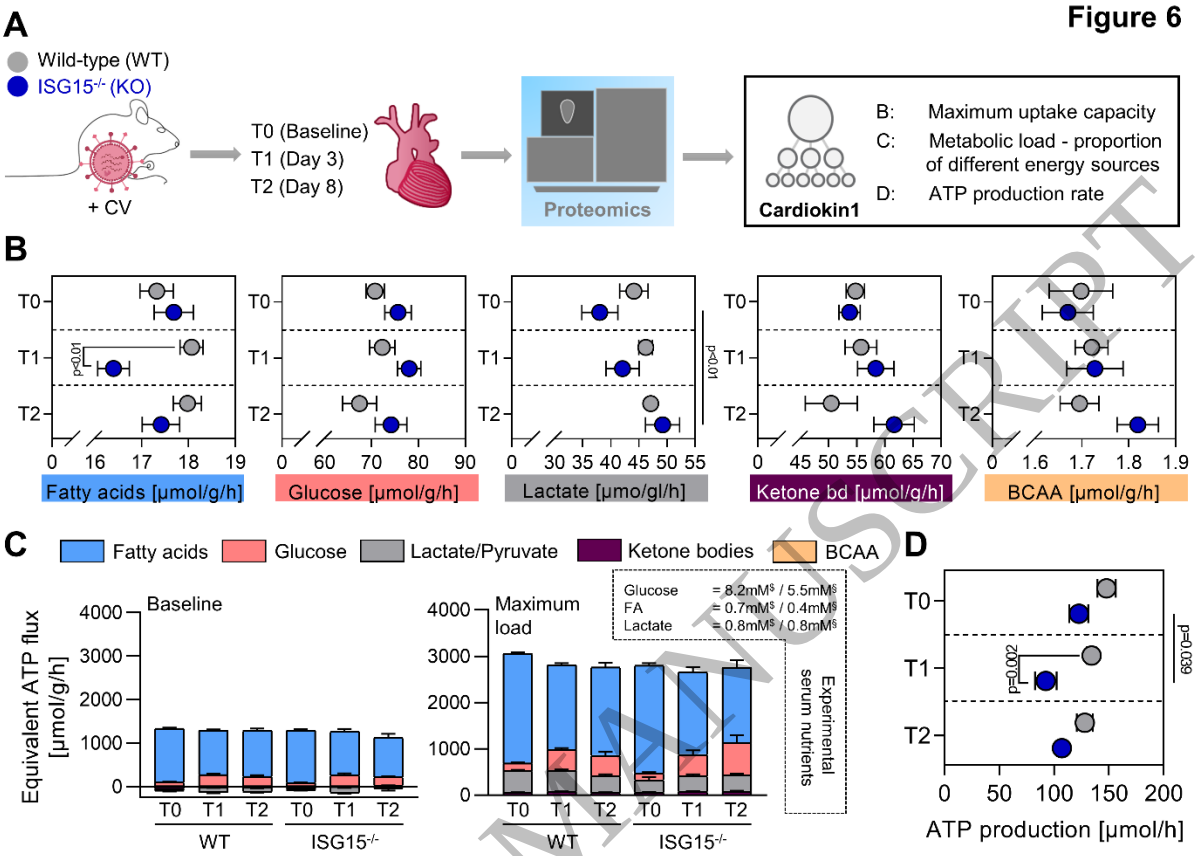

Figure 7

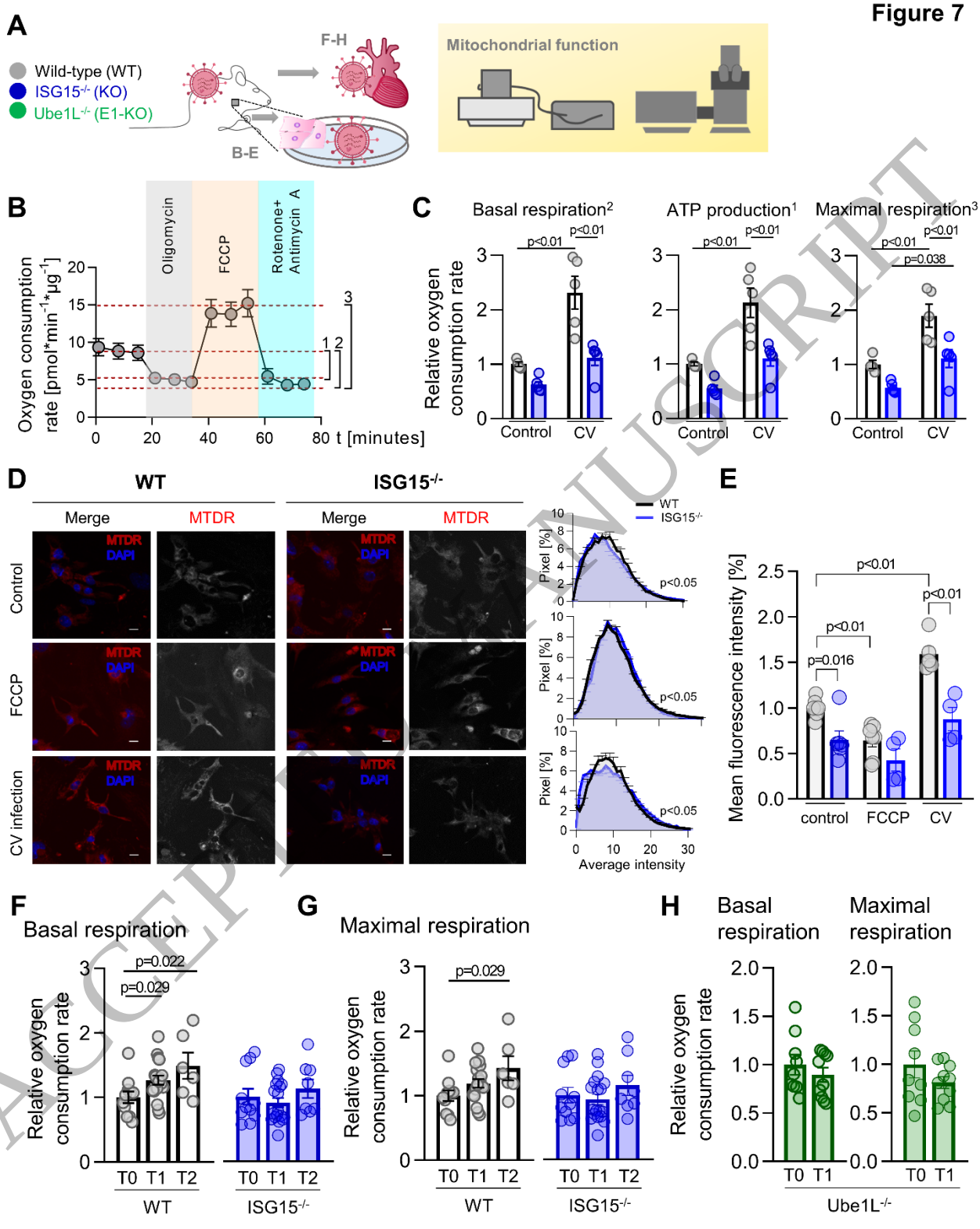

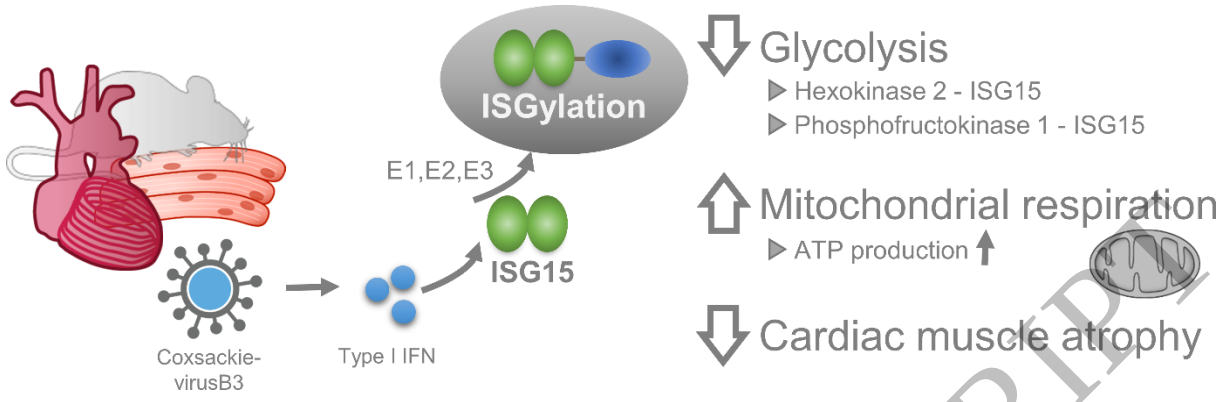

Graphical Abstract

160x51 mm (x DPI)